

Supplementary Information

Self-Discharge of Magnesium-Sulfur Batteries Leads to Active Material Loss and Poor Shelf Life

Hunter O. Ford^a, Emily S. Doyle^a, Peng He^a, William C. Boggess^b, Allen Oliver^b, Tianpin Wu^c,

George E. Sterbinsky^c, Jennifer L. Schaefer^{*a}

a. Department of Chemical and Biomolecular Engineering, University of Notre Dame, Notre Dame, IN 46556, USA. *E-mail: Jennifer.L.Schaefer.43@nd.edu

b. Department of Chemistry, University of Notre Dame, Notre Dame, IN 46556, USA.

c. X-ray Science Division, Advanced Photon Source, Argonne National Laboratory, Lemont, IL 60439, USA.

Experimental

Preparation of electrolytes: $MgTFSI_2/MgCl_2$ in DME. This synthesis was conducted within the glovebox unless noted otherwise. Magnesium bis(trifluoromethanesulfonimide) ($MgTFSI_2$) (Solvionic) is dried at 200 °C under vacuum on a Schlenk line, and then transferred to an argon filled glovebox. Within the glovebox, the $MgTFSI_2$ is dissolved in 1,2-dimethoxyethane (DME, 99.5% inhibitor free, Aldrich), that had been stored on activated 3 Å molecular sieves (Aldrich) for at least 3 days, to form either a 0.25 M solution or 1 M solution, depending on the concentration of the electrolyte. After dissolving the $MgTFSI_2$, magnesium chloride ($MgCl_2$) beads (anhydrous, beads, 99.99% Aldrich) were added to the solution to yield either a 0.5 M or 2 M $MgCl_2$ solution ($MgTFSI_2:MgCl_2$ is 1:2). This procedure was completed according to the literature.¹ The resulting solution was stirred until the $MgCl_2$ had reacted and fully dissolved. The $MgTFSI_2/MgCl_2$ DME solution is then stirred on molecular sieves for at least 24 h prior to use.

$MgHMDS_2/AlCl_3$ in THF. This synthesis was conducted within the glovebox unless noted otherwise. Magnesium bis(hexamethyldisilazide) ($MgHMDS_2$) (97%, Aldrich) was recrystallized from heptane (anhydrous, 99%, Aldrich) within an argon filled glovebox by adding to heptane, heating until dissolved, then cooling the heptane to precipitate crystallization. The $MgHMDS_2$ was collected by filtration. For 2.5 mL scale, 0.302 g recrystallized $MgHMDS_2$ were dissolved in 0.9 mL of tetrahydrofuran (THF, anhydrous, 99.9%, inhibitor-free, Aldrich) that had been stored on activated 3 Å molecular sieves for at least 3 days. 0.2335 g aluminum chloride ($AlCl_3$, anhydrous, 99.99%, Aldrich) were dissolved in 1.9 mL THF incrementally. The $AlCl_3$ THF solution was added to the $MgHMDS_2$ THF solution, and the resulting solution was stirred overnight to allow the formation of the active magnesium complex. This solution is 0.35 M with respect to magnesium, with a 1:2 molar ratio $MgHMDS_2:AlCl_3$.

$MgFPB$ in DEG. This synthesis was conducted according to the literature entirely within the glovebox unless noted otherwise.² First, 100 mL of DME dried on sieves were stirred over Na metal. The DME and the metal surface turned orange, and the Na was cut to expose fresh Na. This was repeated until the surface of the newly exposed Na did not change in appearance. The DME was then distilled under N_2

using standard Schlenk techniques to avoid exposure to water and oxygen, yielding a clear colorless solvent. 2.81 g of hexafluoro-2,3-bis(trifluoromethyl)-2,3-butanediol (hbtp, TCI, 98%) were dissolved in 5 mL of the purified DME, liberating a small amount of vapor. Separately, 108 mg of MgBH_4 (95%, Aldrich) were suspended in 20 mL of the purified DME. The 5 mL of hbtp solution were added slowly and dropwise to the suspended MgBH_4 in DME, liberating H_2 . After stirring overnight, this colorless and slightly cloudy solution was transferred to the Schlenk line, and then concentrated to about 5 mL under vacuum. The concentrated solution was brought back into the glovebox, then charged with 30 mL of hexane (anhydrous, 99%, Aldrich). The formation of two phases was noted, a viscous liquid phase about 4 mL at the bottom of the flask, and a top liquid phase. The top phase was removed, and the viscous phase was washed twice more with 10 mL of hexane. The viscous phase was dried under high-vacuum to yield a very fine white powder, the magnesium fluorinated pinacolatoborate (MgFPB) salt. This powder was then dried under dynamic vacuum overnight at room temperature.

For a 0.5 M solution, 1.37 g of MgFPB were dissolved in 2 mL of diethylene glycol dimethyl ether (DEG, anhydrous, 99.5%, Aldrich) that had been purified with sodium in the same way the DME above was purified, the only difference being that the DEG was distilled under vacuum instead of N_2 . The resulting solution was colorless and slightly cloudy. The MgFPB solution was charged with 100 mg of magnesium powder (325 mesh, 99.8%, Alfa Aesar) then parafilm and stirred in a 50 °C oil bath. After stirring for 24 h, the solution was filtered, rendering it ready for use.

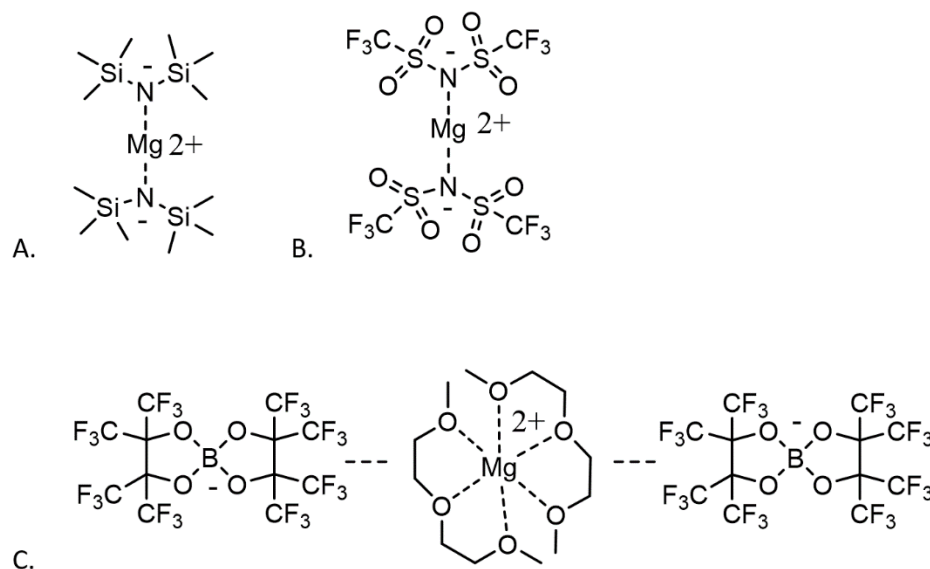


Figure S1. Chemical structures of electrolyte salts. A. MgHMDS_2 B. MgTFSI_2 C. $\text{MgFPB} \cdot \text{DME}_2$

Synthesis of magnesium polysulfides

The Mg polysulfide solution was prepared by mixing Mg powder and S powder (99.98%, Aldrich) in the 0.25 M MgTFSI_2 + 0.5 M MgCl_2 DME electrolyte that had been stored on sieves. The electrolyte was

filtered before use. The Mg powder (2 mg), S powder (16 mg) and electrolyte (2 mL) were added into a 20 mL vial with a small stir bar. The mixture was stirred for 2 h under room temperature until the solution turned light orange. After that, the vial was sealed with Teflon tape and parafilm. The solution was stirred overnight at 50 °C, deepening in color. After filtration, the magnesium polysulfide solution was ready for analysis. The nominally 0.2 M (in terms of atomic S) solution is synthesized first, from which the 0.05 M solution is produced via dilution with additional electrolyte. This synthesis protocol was repeated for synthesizing magnesium polysulfides in the MgFPB and MgHMDS₂/AlCl₃ electrolytes.

Electrochemical measurements

Mg-S cathodes were prepared by punching activated carbon cloth (FM100, double-weave, Charcoal House) into 3/8" diameter disks. Inside an argon filled glovebox, 0.76 mg of S were added to each carbon disk to yield 1 mg S/cm². This was accomplished by dissolving the appropriate amount of sulfur in sieve-dried THF, then adding 60 µL of this solution to the cathode in 15 µL increments, 30 µL on each side. The THF was evaporated by allowing the cathodes to sit in the open atmosphere of the glovebox. Then, the cathodes were loaded into a Chemglass glass pressure vessel, sealed, then heated at 155 °C for 12 h within the glovebox oven to melt infuse the sulfur into the carbon cloth yielding ACC-S.

Magnesium metal (99.9%, 0.1 mm thick, MTI corp.) was punched into disks, from which the oxide layer was removed via scraping. 2032 type coin cells were assembled with Mg anode, separator, ACC-S housed in a Teflon spacer (1/32" thick, McMaster Carr), 160 µL of electrolyte added to the ACC-S, stainless steel spacers, wave spring. All cells used one 3/4" diameter Celgard 2325 separator unless otherwise noted. Cells with the 1 M MgTFSI₂ + 2 M MgCl₂ DME electrolyte used one 3/4" diameter glass fiber separator (200 °C vacuum dried, Whatman), as this electrolyte does not wet Celgard.

Assembled cells were rested for an appropriate amount of time (cells that were not aged for a time specified in the manuscript were rested for 1 h), then discharged at a rate of 0.1C with respect to sulfur loading using a Neware Battery Tester unless otherwise noted. Discharge was controlled on the basis of potential or capacity, as appropriate.

Lithium-sulfur cells for mass spectrometry technique validation were prepared as follows. Sulfur powder and disordered mesoporous carbon (ACS material, surface area 600 m²/g) were combined in an 80:20 sulfur:carbon mixture, thoroughly ground together with mortar and pestle, loaded into a sealed glass pressure vessel and heated at 155 °C for 12 h within the glovebox oven. This resulting S/DMC, super P conductive carbon (MTI corp.), and polyvinylidene fluoride (Arkema) were combined in an 80:10:10 ratio with N-methylpyrrolidone (NMP) and stirred for 24 h. The resulting slurry was cast on carbon coated aluminum (MTI corp.) using a doctor blade, which was then dried at 55 °C for 12 h. Cathodes were punched from this material in 3/8" diameter, with loadings of 1.1 – 1.5 mg S/cm². Lithium foil (Alfa Aesar, 0.75 mm thick, 99.9%) was polished to a reflective shine by removing the oxide layer, then cut into 3/8" diameter electrodes. Cells were assembled with the cathode, Celgard 2325 separator, and Li anode. Electrolyte, 1 M LiTFSI (TCl, >98.0%, dried in dynamic vacuum 120 °C for 12 h) dissolved in sieve dried 1,3-dioxolane (DOL):DME 1:1 v/v, was restricted to 20 µL electrolyte / mg S and was added to the

cell during assembly. Cells were rested for 1 h, then discharged to 2.2 V. Cells were derivatized for UPLC-MS in the same way as Mg-S cells.

Cyclic voltammetry was carried out using a PARSTAT MC-1000 potentiostat/galvanostat (Princeton Applied Research), where the magnesium electrochemistry of the various electrolytes was evaluated within 2032 coin cells using a magnesium counter/reference electrode and stainless steel working electrode. The potential was swept at a rate of 10 mV/s.

Electrochemical impedance spectroscopy was also carried out on the same PARSTAT-MC-1000 workstation, where the frequency was swept from 1,000,000 Hz to 0.1 Hz with an amplitude of 5 mV RMS.

Preparation of UV/VIS samples

Coin cells that had been discharged and aged or aged at OCP as appropriate were opened within the glovebox, and the cathodes were recovered and placed into 400 μ L of sieve-dried THF for 5 min. The choice of THF as an extraction solvent for preparing the UV/VIS samples was one informed by economics and compared to using the electrolyte as an extraction medium should not alter the conclusion of the UV/VIS experiments. The resulting solution was collected, filtered through 0.45 μ m syringe filters, and added to 1 mm path-length quartz cuvettes (Type 30 Standard Micro Cuvette with PTFE stopper, Firefly Sciences). The reference/background solution for each electrolyte type was prepared by assembling a full Mg-S cell using that electrolyte, resting it for 1 h plus the total amount of time required to discharge an identical cell to 200 mAh/g (about 2 additional h), then preparing it as described above. This ensures that the background subtraction solution contains the same concentration of solvent and salts as the sample solutions being analyzed. Therefore, everything observed in the UV/VIS spectrum is a result of a chemical/electrochemical reaction. The reference for the synthesized Mg polysulfides is the pristine electrolyte used for the synthesis. The cuvettes are sealed within the glovebox, and then analyzed using a Jasco V-670 UV-Visible-Near IR Spectrometer from 200 cm^{-1} to 650 cm^{-1} .

Preparation of ultra performance liquid chromatography – mass spectroscopy (UPLC-MS) samples

Samples for UPLC-MS were prepared similarly to the sample preparation for the UV/VIS samples. In a typical analysis, a coin was opened within the glovebox, with the cathode and separator recovered and added to 400 μ L of sieve-dried DME for 30 s. The DME was removed, then replaced with fresh DME twice. The cathode and separator were then transferred to a solution of 5 mg of 4-(dimethylamino)benzoyl chloride (DBC) (>99.0%, for HPLC derivatization, Aldrich) suspended in 100 μ L of sieve dried DME. The DBC quickly reacts with solid (poly)sulfides in the cathode and separator, yielding a clear yellow solution (Figure S33). After 5 min, this solution was removed from the glovebox and charged with 200 μ L of 66:34 by vol acetonitrile (ACN):water (both HPLC grade) both with 1 mM ammonium acetate. After filtration, the clear slightly-yellow solution was analyzed with UPLC-MS. If no polysulfides were present in the cathode, the solution remained colorless and the DBC did not dissolve until the addition of the ACN:water.

A Waters Acquity UPLC system consisting of a sample manager and binary solvent manager was used to inject 20 μL of sample with water:ACN 90:10 v/v 1 mM ammonium acetate onto a Waters Acquity UPLC BEH C18 column (1.7 μm , 2.1 x 100 mm) at a flow rate of 0.4 mL/min. Column temperature was maintained at 40 °C. During the 20 min operation, the gradient used is as follows: 90% water, 10% acetonitrile for 2 min, then gradient transition to 100% ACN by 19 min, after which there was a gradient transition back to the 90:10 water:ACN ending at 20 min. A t-split was used to deliver 50% flow from the column to the mass spectrometer.

For MS detection, a Waters Acquity TQD Triple Quadrupole was operated in ESI+ mode with the following parameters: capillary 3.2 kV, cone 15 V, extractor 3 V, RF lens 0.1 V, source temp 150 °C, desolvation temp 350 °C. Nitrogen flow is 650 L/h for desolvation, 50 L/h for cone. From the mass spectrum, the masses corresponding to the di-functionalized polysulfides (refer to scheme 1) were detected as a function of retention time. All of the parameters were chosen to maximize analyte signal. Using the Acquity software, the area under the peaks associated with each polysulfide was integrated and recorded. By summing these areas (multiplied by the number of sulfur atoms present in each species), the total ionic sulfur on the basis of sulfur atoms was calculated.

Error was calculated in the following way. Firstly, sets of samples were prepared in triplicate, one set containing a large amounts of solid ionic polysulfides and one containing amounts near the instrument detection limit. From the quantitative results for total sulfur content in these samples, relative standard deviations were calculated and appropriately applied to the data shown in Figure 3 and Figure S26. Additionally, error from noise and non-analyte ions of matching m/z was calculated by obtaining the area in the chromatogram to either side of the analyte peak, over a period of total integration that matches the analyte peak. For example, if the analyte peak was centered at 2.0 min and was 0.5 min wide, the area from 1.5 min to 1.75 min was summed with the area from 2.25 min to 2.5 min and applied as additional error to the result.

SEM-EDX

Samples were sealed inside a vacuum transfer chamber (PELCO SEM Pin Stub Vacuum Desiccator) for transfer to the SEM facility. Electronically conductive samples were transferred directly from the vacuum chamber into the SEM (Magellan 400 XHR FESEM, equipped with an Everhart-Thornley SE detector and Bruker EDX spectrometer). Non-conductive samples were sputter coated with 2 nm of iridium using a 208HR High Resolution Sputter Coater (Ted Pella Inc.), then transferred into the SEM. All care to minimize sample exposure to air was taken, but it was impossible to completely avoid air exposure. Samples were analyzed at a working depth of 5 mm, with an operating voltage of 10 kV and current density of 1.6 nA.

Estimation of sulfur solubility

A small amount of sulfur powder, 1.0 – 1.5 mg, was measured into a vial. To the vial, the solution to be tested was added in 10 μL increments. The vial was then shaken for at least 1 min, and if sulfur powder was still visible, another increment was added. The ending volume when sulfur particulate could no longer be seen was used in conjunction with the original mass of sulfur to estimate the solubility.

Powder X-ray diffraction

The sample was collected in a 0.5 mm borosilicate capillary and mounted on a Bruker Photon-II diffractometer. The specimen was centered to rotate along the phi-axis of the instrument. The sample to detector distance was set to 150.0 mm. Data were recorded with Cu-K α radiation at room temperature. Five frames at varying 2-theta angles, each exposed for 60 s with a phi-360° rotation applied to the sample, were recorded. These were composited within APEX-III software and the intensities integrated across the Laue rings to produce the PXRD diffractogram. The effective data range is 5 to 90° in 2-theta, with an effective step size of 0.02° in 2-theta. Spectra were background subtracted as appropriate.

Synchrotron X-ray absorption spectroscopy (XAS)

Cells containing the 0.25 M MgTFSI₂ + 0.5 M MgCl₂ in DME electrolyte were assembled, discharged to 200 mAh/g, and then aged for 168 h, producing the solid magnesium polysulfide precipitate. These cells were opened, the separator containing the deposit was harvested and washed with anhydrous THF, then dried. Standard coin cells were modified by drilling a ¼" diameter hole in the bottom of the case. A ¾" diameter punch of Kapton film (7.5 μ m thick, Premier Lab Supply, Premier Thin Film TF-475 Kapton Continuous Roll) was super glued to the inside of the case, making the cell air-tight but allowing for X-ray penetration to the sample. The separator with target sample was loaded into the cell, with the sample facing the Kapton window. The cell was sealed with two stainless steel spacers, wave spring, and unmodified top case. An example of a prepared cell can be seen in Figure S13. A reference S₈ sample was prepared in the same manner, but by mixing 1 wt% sulfur powder with 99 wt% cellulose powder as the target.

Samples were measured at beamline 9-BM of the Advanced Photon Source at Argonne National Laboratory. The incident energy was selected with a Si(111) double crystal monochromator, and a rhodium coated mirror was used to reject higher order harmonics. Samples were analyzed in a helium-purged chamber, and the monochromator energy was calibrated to the S₈ reference. The absorption spectra were obtained by collecting the sulfur K α fluorescence as a function of incident energy using a four element silicon drift detector and dividing this by the incident intensity that was monitored by a helium filled ion chamber. Using Athena XAS data processing software, the collected spectra were signal averaged, normalized, and displayed as total fluorescence intensity or Fourier transform magnitude. The spectra were normalized by first subtracting a line that was fit to the pre-edge region below the onset of the white line and then division by a constant such that the post edge intensity is roughly equal to one. Before Fourier transformation, the background was modeled by a spline function and subtracted from the normalized spectrum and energy was converted into photoelectron wavenumber using an E_0 of 2470.4 eV. A window from 3 to 7 \AA^{-1} was used for Fourier transformation.

Nuclear magnetic resonance spectroscopy

The magnesium polysulfide precipitate, embedded in a Celgard separator, was immersed into deuterated DMSO (Aldrich) within the glovebox, immediately resulting in a blue solution. The sample

was transferred to a NMR tube, which was capped and sealed with parafilm, then analyzed on a Bruker 400 MHz NMR spectrometer. Data was processed with Bruker TopSpin software.

Further supporting figures

Plating/stripping of Mg in studied electrolytes

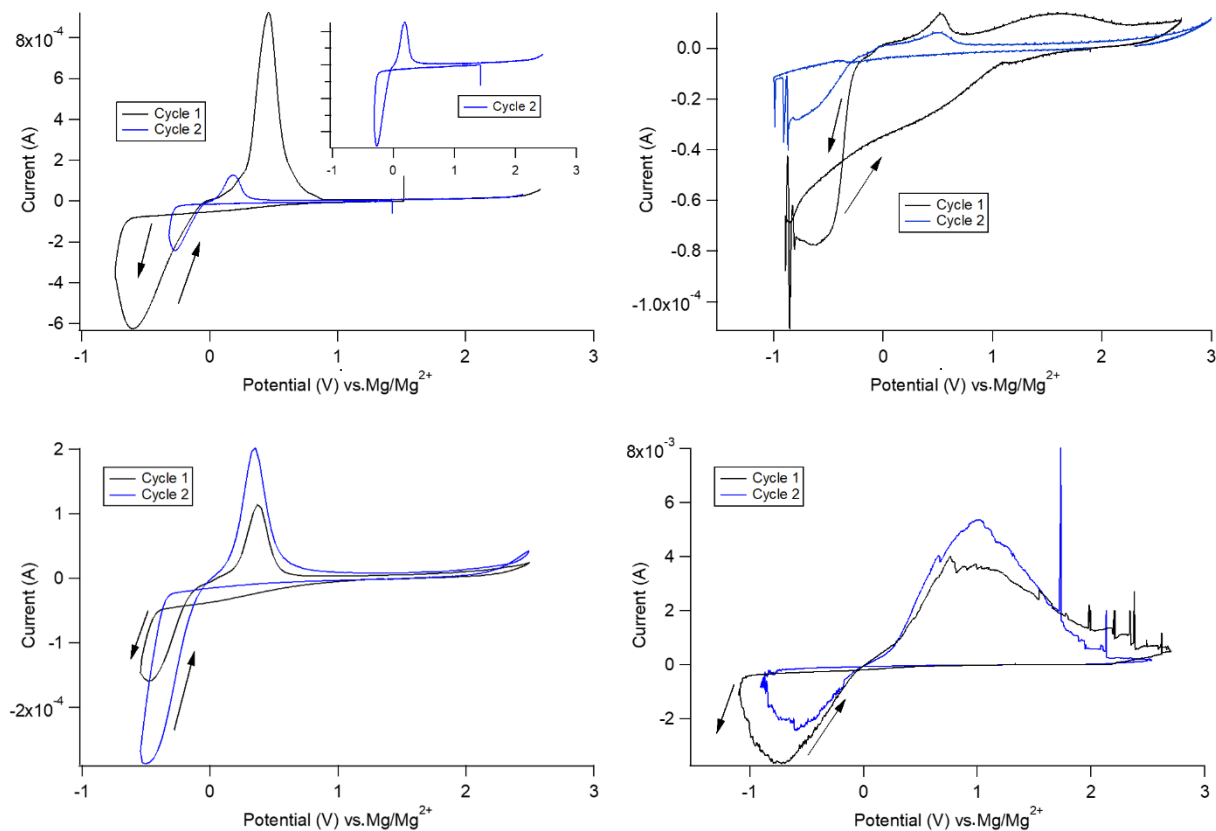


Figure S2. CVs for the four different magnesium electrolytes used in this study. Top left: 0.25 M MgTFSI₂ 0.5 M MgCl₂ in DME. Top right: 1 M MgTFSI₂ + 2 M MgCl₂ in DME. Bottom left: MgHMDS₂ + AlCl₃ in THF. Bottom right: 0.5 M MgFPB in DEG. CVs are done in two electrode configuration coin cells, using 100 μ L of un-conditioned electrolyte, magnesium counter/reference and stainless steel working electrodes at a rate of 10 mV/s.

Figure S2 shows CVs on the studied electrolytes. The overall efficiency and the deposition/stripping overpotential differ for each electrolyte, with each electrolyte showing changes in these parameters from cycle 1 to cycle 2. Of note is that the current density of the MgFPB electrolyte is about an order of magnitude higher than that of the other three electrolytes, the reason for which is unknown at this time. The figures above show each electrolyte, while perhaps not the most efficient, is at least capable of magnesium electrochemistry.

Additional SEM-EDX images

Figures S3 – S7 contain additional SEM-EDX images of deposits found on the separator and cathode of a Mg-S cell with a 0.25 M MgTFSI₂ + 0.5 M MgCl₂ DME electrolyte, discharged to 200 mAh/g, then aged 168 h. Figures S6 and S7 show how the morphology and elemental composition of the electrolyte salts differ from those of the deposits observed in Figure 2A and Figures S3, S4, and S5. The lack of Cl, F, and N and difference of structure in Figure 2 and Figures S3, S4, and S5 compared to S6 indicate the deposits in Figure 2A and Figures S3, S4, and S5 are not simply deposits of electrolyte salts.

Figures S8A–D show multiple sulfur-rich deposits and deposits attributed to electrolyte salts for 1 M MgTFSI₂ + 2 M MgCl₂ in DME cells aged 168 h.

Figures S9A–C show multiple sulfur-rich deposits and deposits attributed to electrolyte salts for Mg-FPB cells aged 168 h.

Figures S10A-C and S11A-B show various components of a 168 h aged cell using the MgHMDS₂ + AlCl₃ in THF electrolyte. These SEM images show no sulfur-rich deposits on the anode, but sulfur-rich deposits on the cell separator.

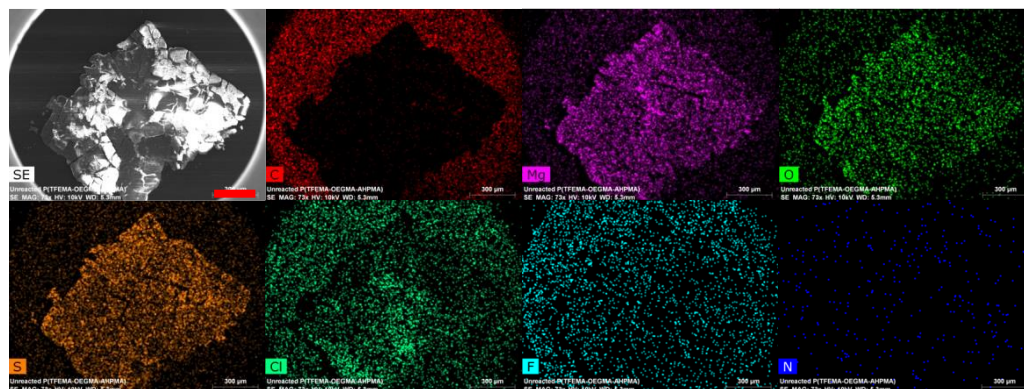


Figure S3. Reproduction of Figure 2 from the main text, but with additional elements as detected by EDX (Cl, F, N). Scale bar is 300 µm.

Table S1. Normalized atom percentages of Mg, O, and S for deposit shown in Figure S3.

Element	[norm. at.%]
Oxygen	35.91876
Magnesium	22.90417
Sulfur	41.17707

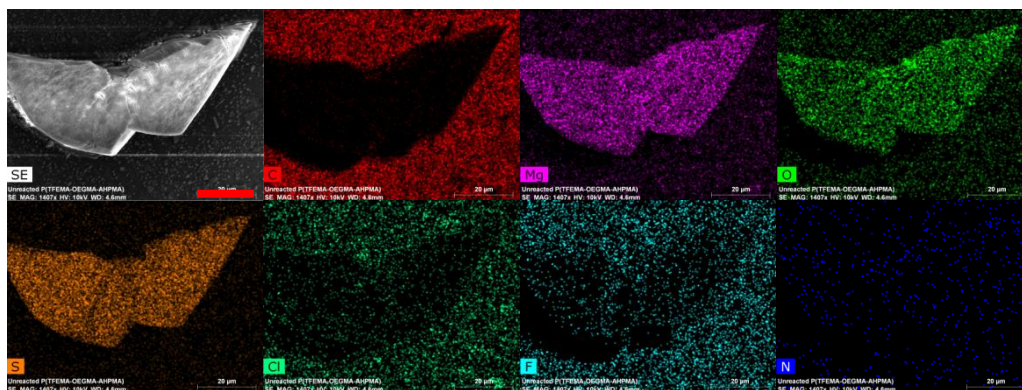


Figure S4. Another deposit on the separator that is primarily Mg, S, O. Scale bar is 20 μm .

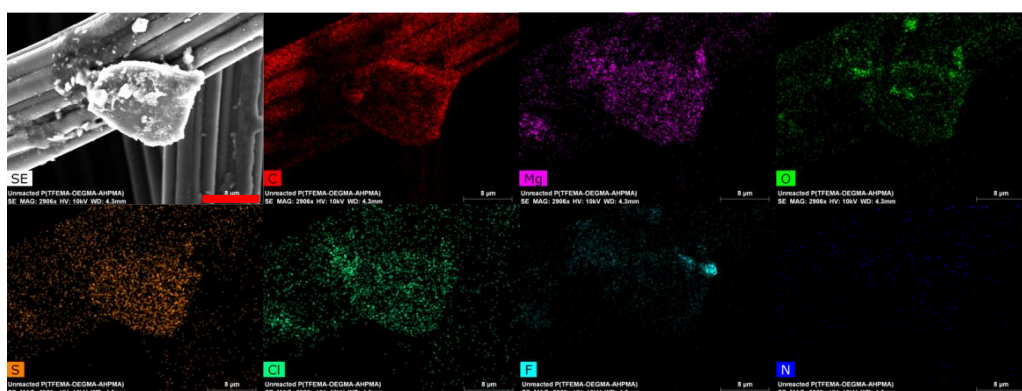


Figure S5. A deposit on the ACC-S cathode that is primarily Mg, S, O, with some C, Cl, F, and a small amount of N. Scale bar is 8 μm .

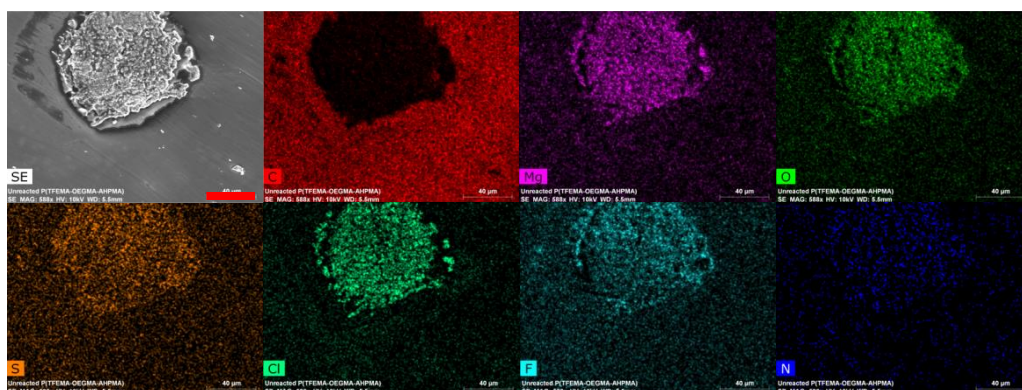


Figure S6. Deposit on separator that is attributed to a combination of the electrolyte salts MgTFSI_2 and MgCl_2 according to the elemental mapping. Scale bar is 40 μm .

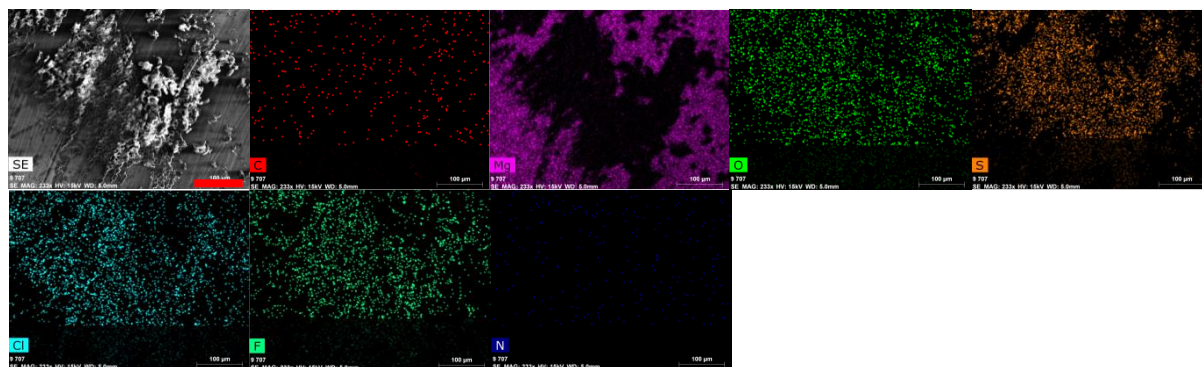


Figure S7 A. SEM/EDX of Mg anode recovered from 0.25 M MgTFSI₂ + 0.5 M MgCl₂ in DME cell showing deposits attributed to the electrolyte salts. Scale bar is 100 μm.

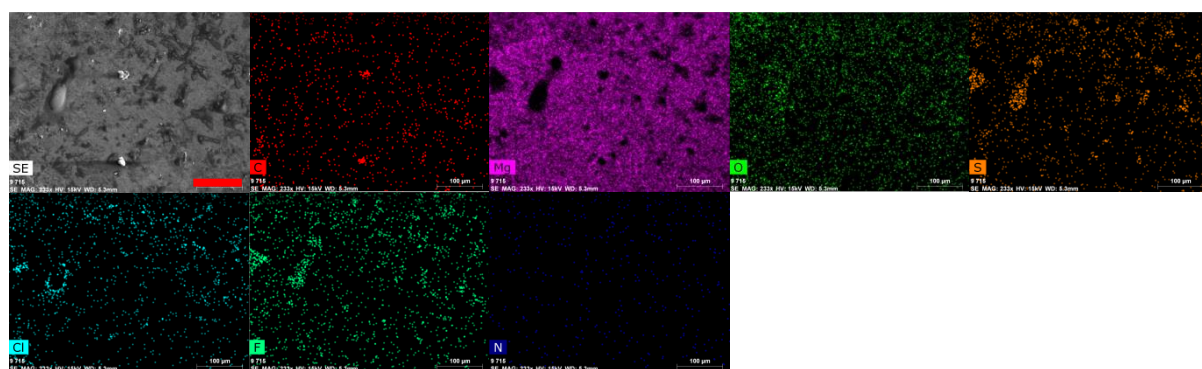


Figure S7 B. SEM/EDX of Mg anode recovered from 0.25 M MgTFSI₂ + 0.5 M MgCl₂ in DME cell showing deposits attributed to the electrolyte salts. Scale bar is 100 μm.

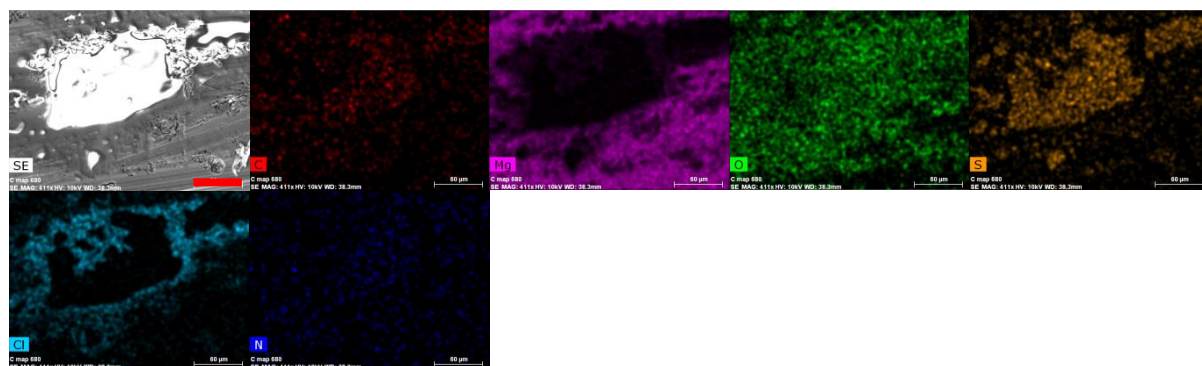


Figure S8 A. SEM/EDX of Mg anode recovered from 1 M MgTFSI₂ + 2 M MgCl₂ in DME cell showing a sulfur-rich deposit. Scale bar is 60 μm.

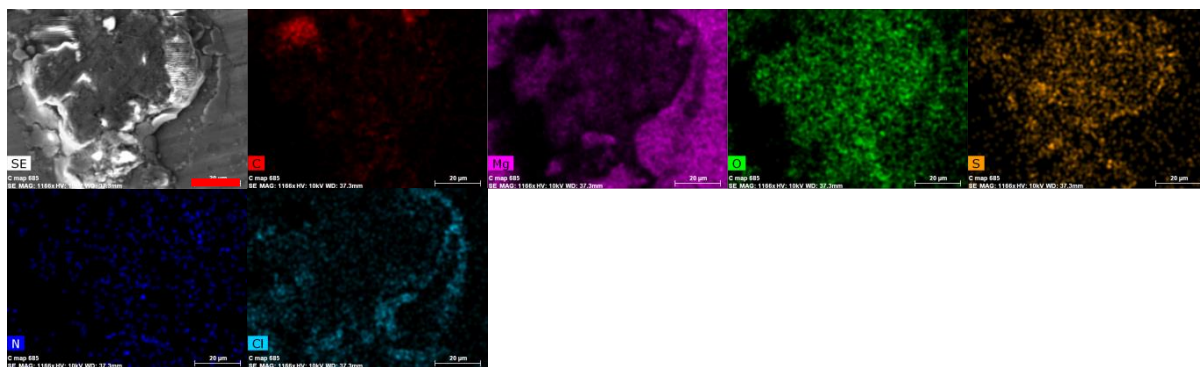


Figure S8 B. SEM/EDX of Mg anode recovered from 1 M MgTFSI₂ + 2 M MgCl₂ in DME cell showing a sulfur-rich deposit. Scale bar is 20 µm.

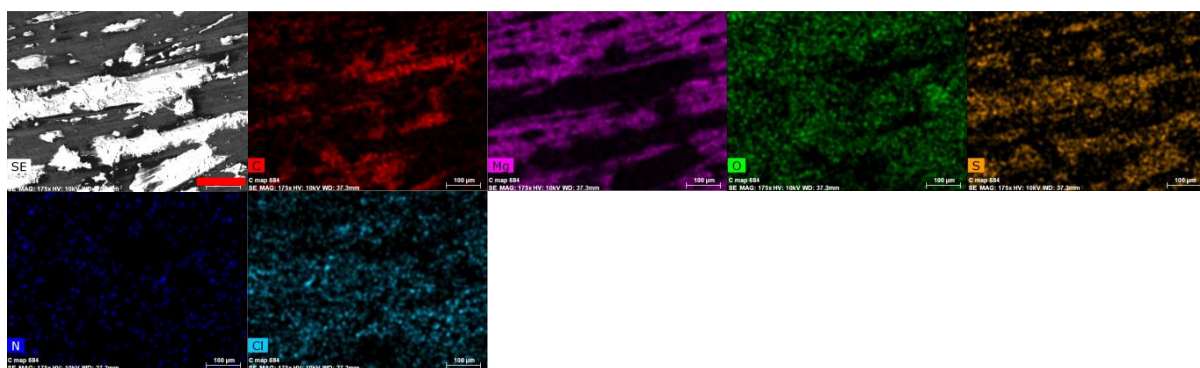


Figure S8 C. SEM/EDX of Mg anode recovered from 1 M MgTFSI₂ + 2 M MgCl₂ in DME cell showing sulfur-rich deposits. Scale bar is 100 µm.

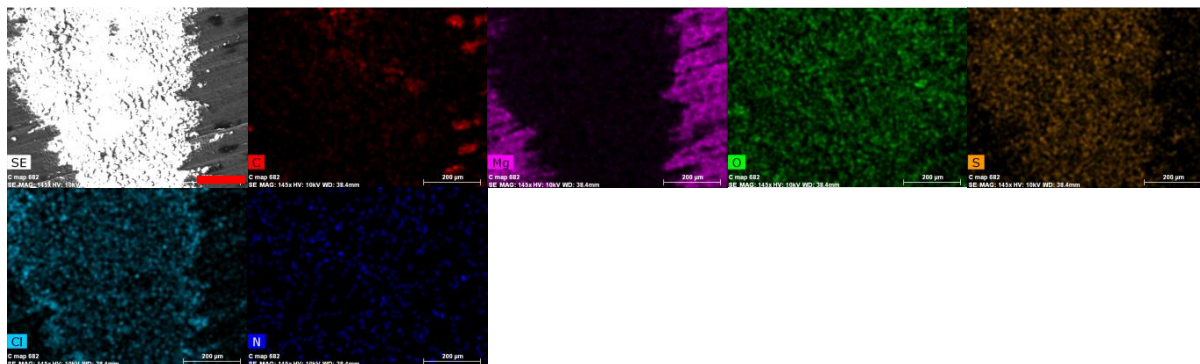


Figure S8 D. SEM/EDX of Mg anode recovered from 1 M MgTFSI₂ + 2 M MgCl₂ in DME cell showing deposits attributed to the electrolyte salts. Scale bar is 200 µm.

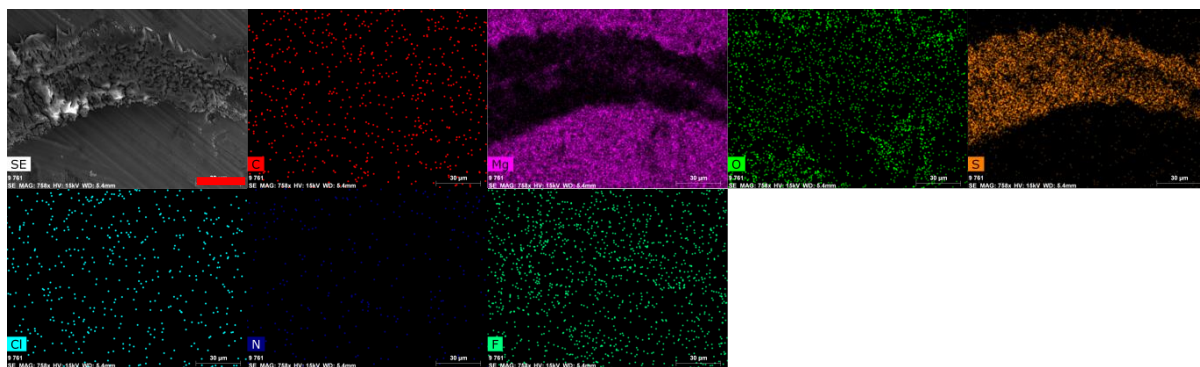


Figure S9 A. SEM/EDX of Mg anode recovered from MgFPB in DEG cell showing a sulfur-rich deposit. Scale bar is 30 µm.

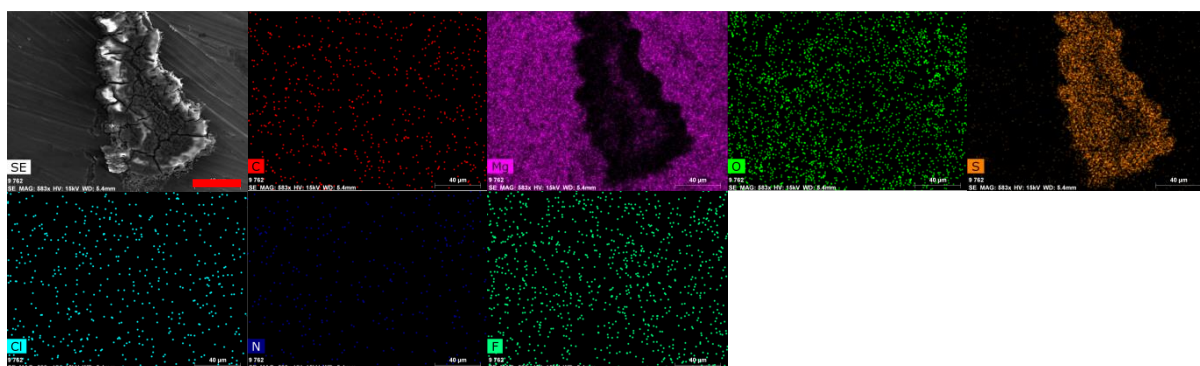


Figure S9 B. SEM/EDX of Mg anode recovered from MgFPB in DEG cell showing a sulfur-rich deposit. Scale bar is 40 µm.

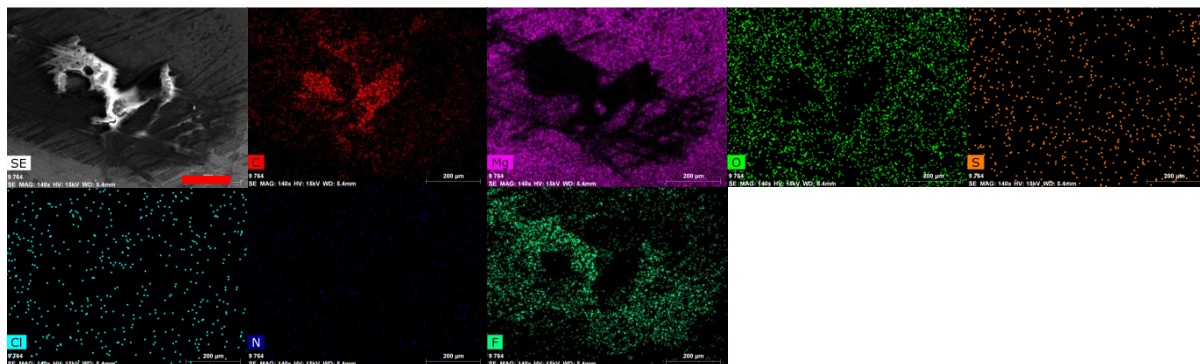


Figure S9 C. SEM/EDX of Mg anode recovered from MgFPB in DEG cell showing deposits attributed to the electrolyte salts. Scale bar is 200 µm.

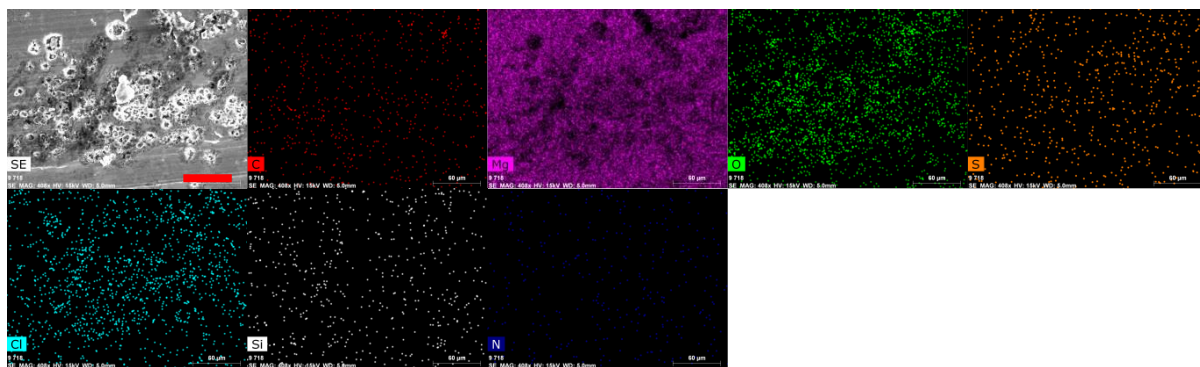


Figure S10 A. SEM/EDX of Mg anode recovered from $\text{MgHMDS}_2 + \text{AlCl}_3$ in THF cell showing pockmarked Mg anode surface. Scale bar is 60 μm .

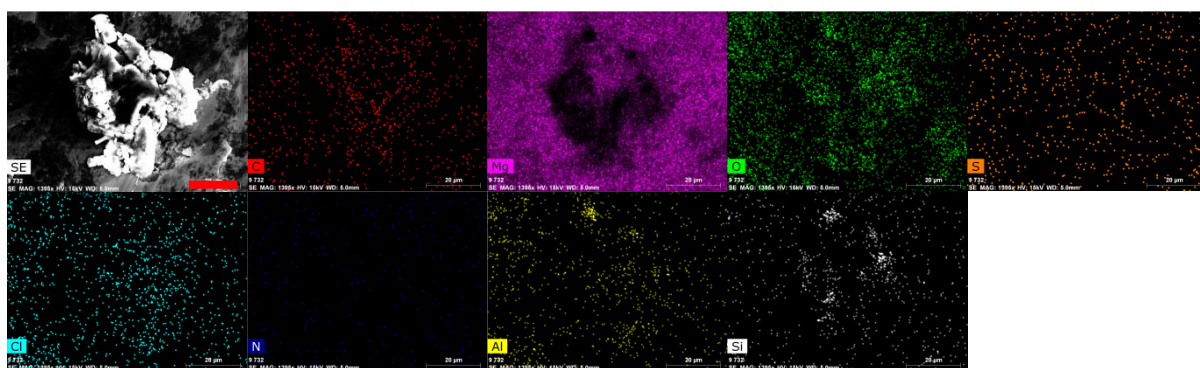


Figure S10 B. SEM/EDX of Mg anode recovered from $\text{MgHMDS}_2 + \text{AlCl}_3$ in THF cell showing MgHMDS_2 salt deposit. Scale bar is 20 μm .

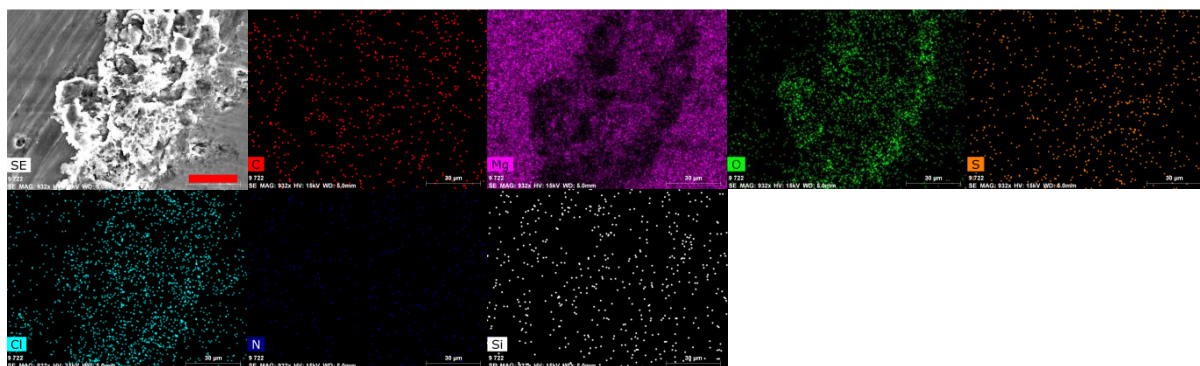


Figure S10 C. SEM/EDX of Mg anode recovered from $\text{MgHMDS}_2 + \text{AlCl}_3$ in THF cell showing Mg and Cl deposit. Scale bar is 30 μm .

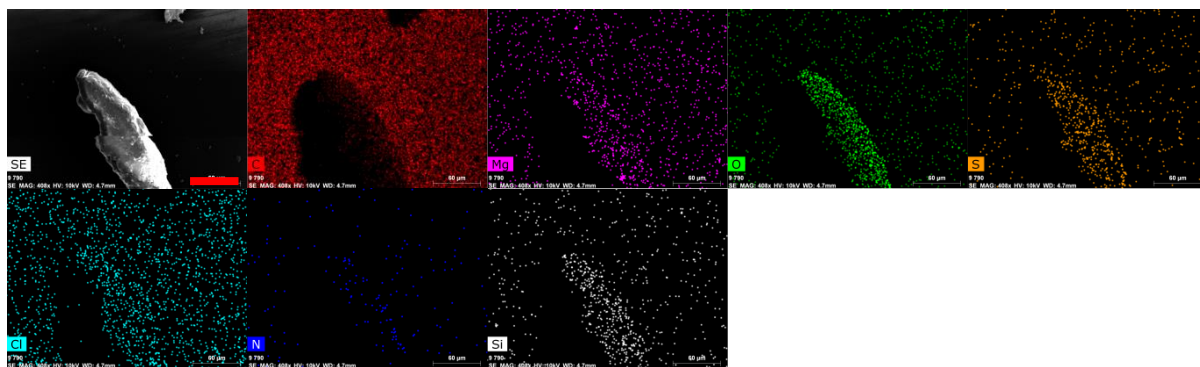


Figure S11 A. SEM/EDX of Celgard separator recovered from $\text{MgHMDS}_2 + \text{AlCl}_3$ in THF cell showing sulfur- and salt-rich deposit. Scale bar is 60 μm .

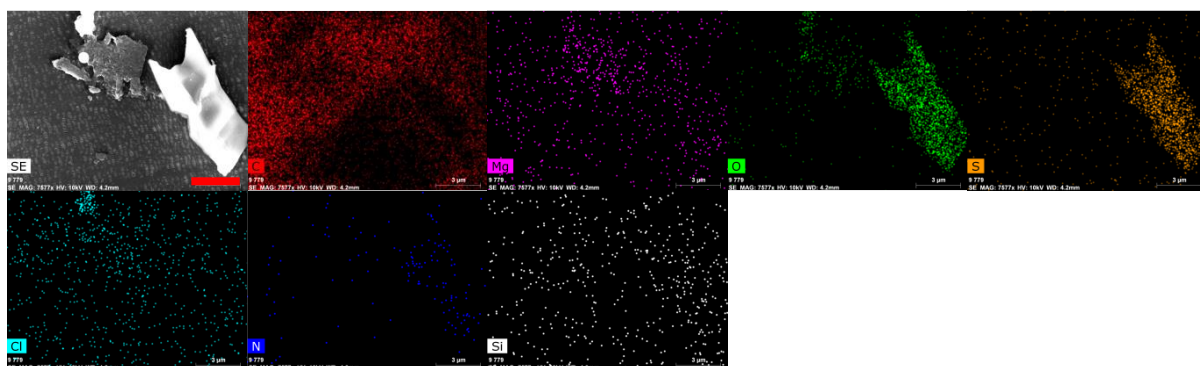


Figure S11 B. SEM/EDX of Celgard separator recovered from $\text{MgHMDS}_2 + \text{AlCl}_3$ in THF cell showing Mg metal chunk (left) and Mg-, O-, S-rich deposit (right). Scale bar is 3 μm .

General comment on SEM/EDX - The figures shown above are representative of the surfaces of the anodes and separators studied; numerous deposits matching those shown above were found on each respective anode. In the cases where no sulfur-rich deposits were found on the anode (0.25 M $\text{MgTFSI}_2 + 0.5 \text{ M MgCl}_2$ and $\text{MgHMDS}_2 + \text{AlCl}_3$ cells), the surface of the anode was scanned for nearly an hour each in search of any S-containing deposits that would represent Mg_xS_y , to no avail. In the cases where anode sulfur-rich deposits were found (1 M $\text{MgTFSI}_2 + 2 \text{ M MgCl}_2$, MgFPB , and separator of $\text{MgHMDS}_2/\text{AlCl}_3$ cells) the sulfur rich deposits were found within about 5 min of studying the surface. Numerous deposits were then subsequently found, indicating the widespread deposition of such compounds.

Further Mg_xS_y solid analysis

Extended X-ray absorption fine structure (EXAFS)

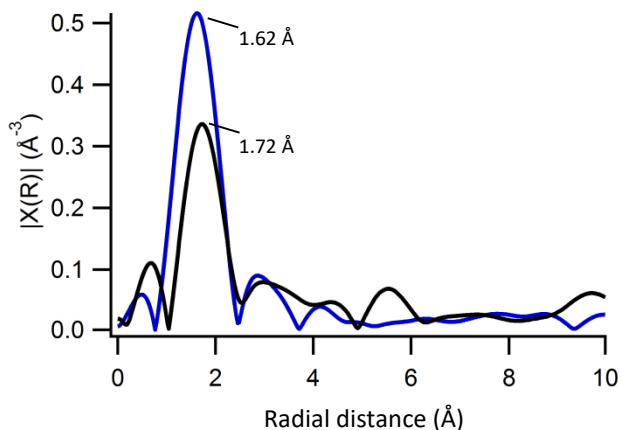


Figure S12. EXAFS data for — Mg_xS_y solid and — elemental sulfur.

As stated in the main text, the max peaks observed in the EXAFS plot are indicative of the geometric environment experienced by the sulfur atoms in the sample. The Mg_xS_y sample analyzed is clearly different from S_8 . From the literature, MgS_8 displays a peak at 1.67 \AA and Mg_3S_8 at 1.30 \AA . The higher the magnesium to sulfur ratio, the more tightly bound the sulfur atoms are within the material. At 1.62 \AA , the Mg_xS_y compound has a magnesium content somewhere between MgS_8 and Mg_3S_8 , which we estimate to be MgS_{6-8} .

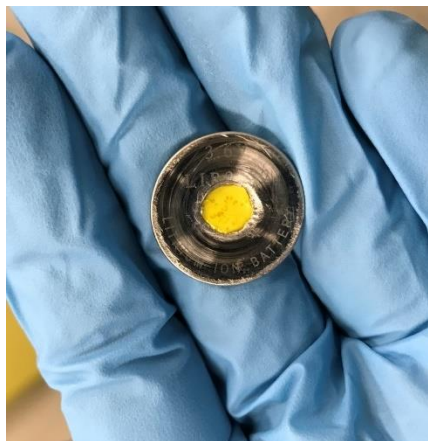


Figure S13. Modified coin-cell with Kapton window for XAS/EXAFS measurement.

Powder X-ray diffraction of Mg_xS_y solid

The M_3S_8 material identified by Xu and colleagues is amorphous; its detection was only accomplished through the use of synchrotron powered X-ray absorption spectroscopy (XAS). PXRD on the material recovered from the separators as shown in Figure 2 reveal that the deposit in our cells is a mixture of amorphous and crystalline phases. The results can be seen in Figure S14.

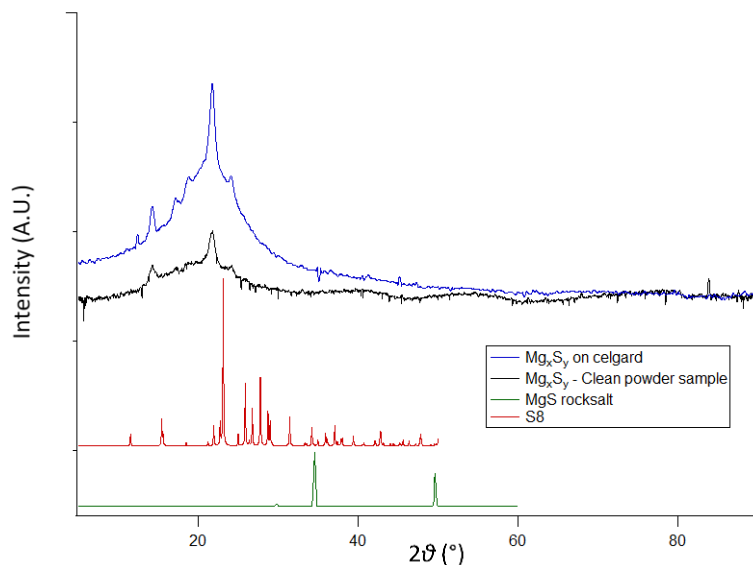


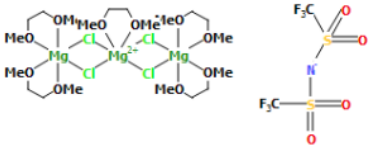
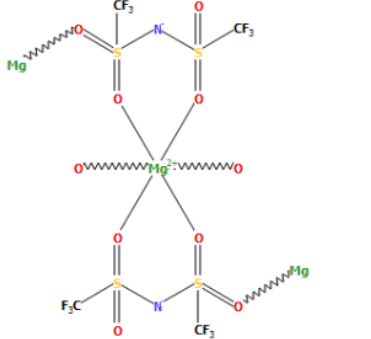
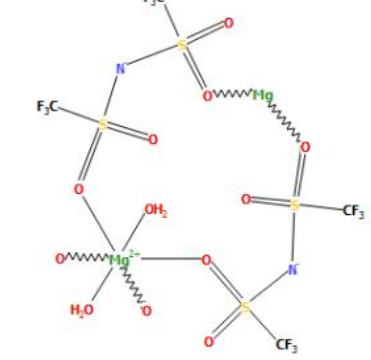
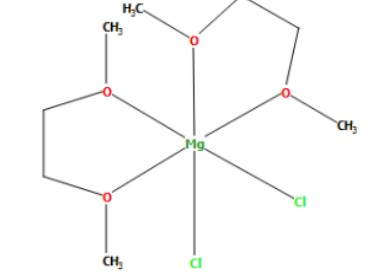
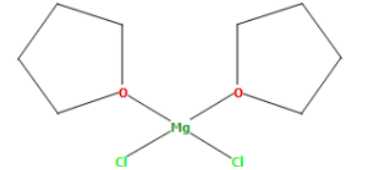
Figure S14. Powder X-ray diffraction for the Mg_xS_y sample obtained from aged 0.25 M $MgTFSI_2$ + 0.5 M $MgCl_2$ in DME cells. Compared against crystalline covalent sulfur S8 and magnesium sulfide.

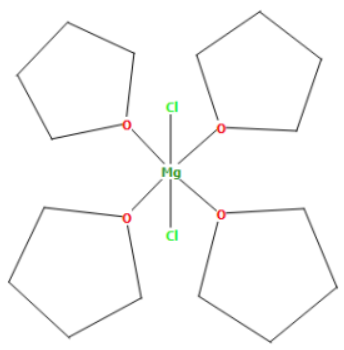
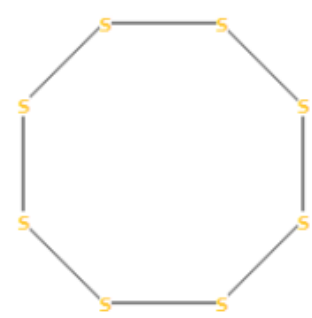
The collection was done in two ways. In the first, the sample was left embedded in the Celgard, which was cut into small pieces and loaded into a capillary. In the second, 8 other separators with the Mg_xS_y deposit were scraped with a razor blade to produce a small amount of the Mg_xS_y powder. This was loaded into the capillary and analyzed. The background subtraction was done such that the influence of the glass capillary and the Celgard separator (if applicable) were removed from the spectra.

An amorphous contribution in the broad hump from $15^\circ - 30^\circ$, over which the crystalline peaks are superimposed, is clearly visible in these diffraction patterns. The multi-component crystalline peaks have been challenging to identify, and likely belong to some previously un-solved solvated complexes containing Mg, Cl, TFSI, DME, and polysulfide. The diffraction peaks do not match any known Mg relevant solvate complexes. Most importantly, the crystalline peaks do not indicate any presence of covalent S8 or other known allotropes of covalent sulfur, nor of magnesium sulfide. The relevant mg solvate complexes examined and the sulfur allotropes are listed in the table below:

Table S2. Crystal structure database identifier, general composition, and structure of compounds relevant for the Mg-S system investigated. None of these have a diffraction pattern matching the pattern in Figure S14.

Cambridge Crystallography Data Centre Database Identifier	General composition	Structure
OGEQAV	Magnesium, chloride, DME, TFSI	

OGEPOI	Magnesium, chloride, DME, TFSI	
QAWWET	Magnesium, TFSI	
QAWWAP	Magnesium, water, TFSI	
WEDCAJ	Magnesium, chloride, DME	
NIVNUB	Magnesium, chloride, THF	

DOVGAW01	Magnesium, chloride, THF	
FURHUV	Sulfur (S8) Shown in Figure S14	
ICSD 659124	Magnesium sulfide, rocksalt Shown in Figure S14	NA

Nuclear magnetic resonance (NMR) on Mg_xS_y solid

Next, the sample was investigated via 1H NMR, with the explicit purpose of determining whether there was bound solvent in the solid product, a common occurrence for magnesium polysulfides.³ For this analysis, deuterated DMSO was chosen as the solvent because it has a high-dielectric constant / donor number and high polysulfide solubility. The thinking was that if there were polysulfides that had precipitated with an ether-based solvent shell, the high donor number DMSO would be able to dissolve that shell and the original solvent would be visible in 1H NMR.

One of the separators that contained the Mg_xS_y powder sample was immersed into deuterated DMSO. Immediately, the solution changed to a vibrant blue color, and all visible solids were dissolved out of the separator. This vibrant blue color is a very characteristic feature of solutions that contain the polysulfide $S_3^{\bullet-}$ radical, and is commonly observed in solutions of Mg polysulfides in DMSO.^{3,4}

This is further direct evidence that the compound is solid magnesium polysulfide. The blue sample is shown below in Figures S15A and S15B. The radical was identified by exposing the solution to water, which results in immediate quenching of the radical anion and a color change to light yellow.

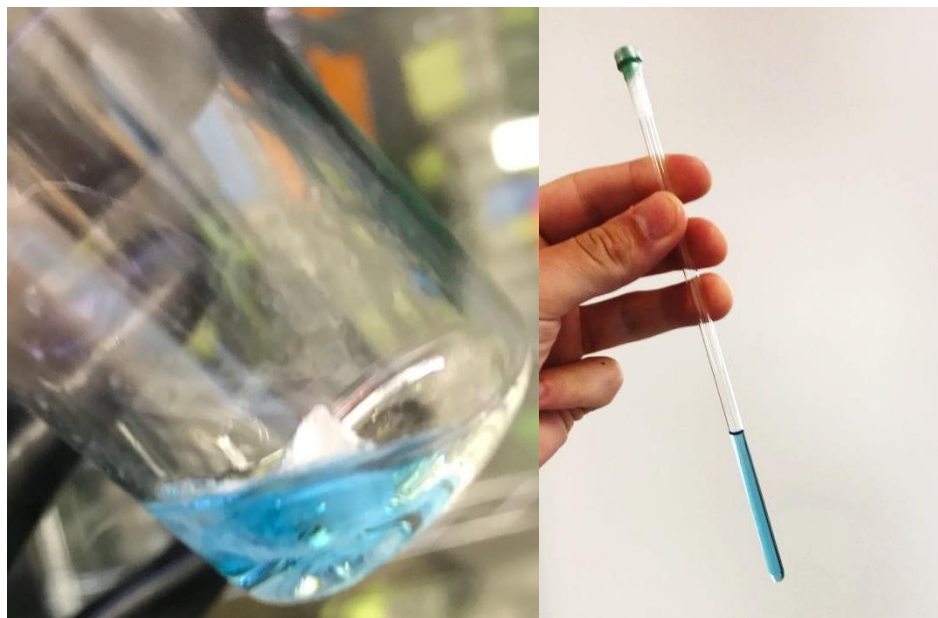


Figure S15A (left). Solution of deuterated DMSO + separator that contained the Mg_xS_y solids. **S15B (right)** shows the solution in an air-tight NMR tube for 1H analysis. The blue color stems from the presence of the ionic polysulfide $S_3^{\bullet-}$.

The results of the 1H NMR are shown below in Figure S16A and S16B. The spectrum shows a very clean sample with only a few peaks. The two singlets at 3.43 ppm (4 H) and 3.24 ppm (6 H) are unmistakably DME, with the 6H signal belonging to the methoxy protons and the 4H signal belonging to the chemically identical aliphatic protons.⁵ The signal at 3.33 ppm is water, 2.50 ppm is residual non-deuterated DMSO, and the tiny multiplets at 3.5 ppm and 1.7 ppm are THF.

The separator from which this sample was prepared was dried for over 9 h in the glovebox after its initial rinsing with THF (per standard procedure to remove salts and solvent besides the Mg_xS_y deposit), prior to its NMR analysis. The DME must be locked into the solid material, otherwise its signal would be of similar magnitude to the THF due to evaporation. These results indicate that the Mg_xS_y precipitate contains DME solvent molecules in its structure.

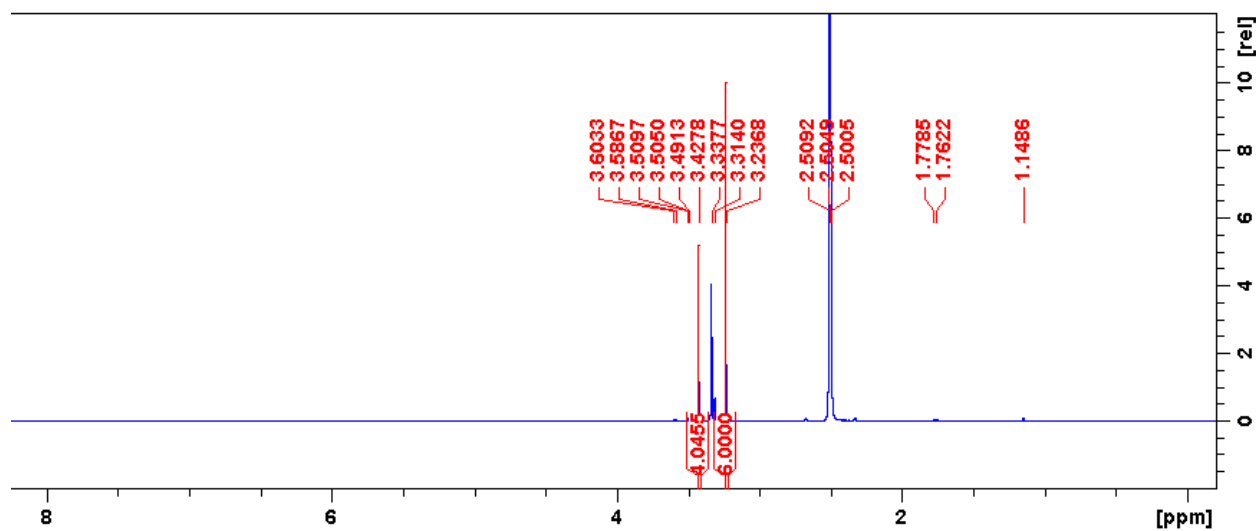


Figure S16A. ^1H NMR results for the DMSO dissolved Mg_xS_y sample.

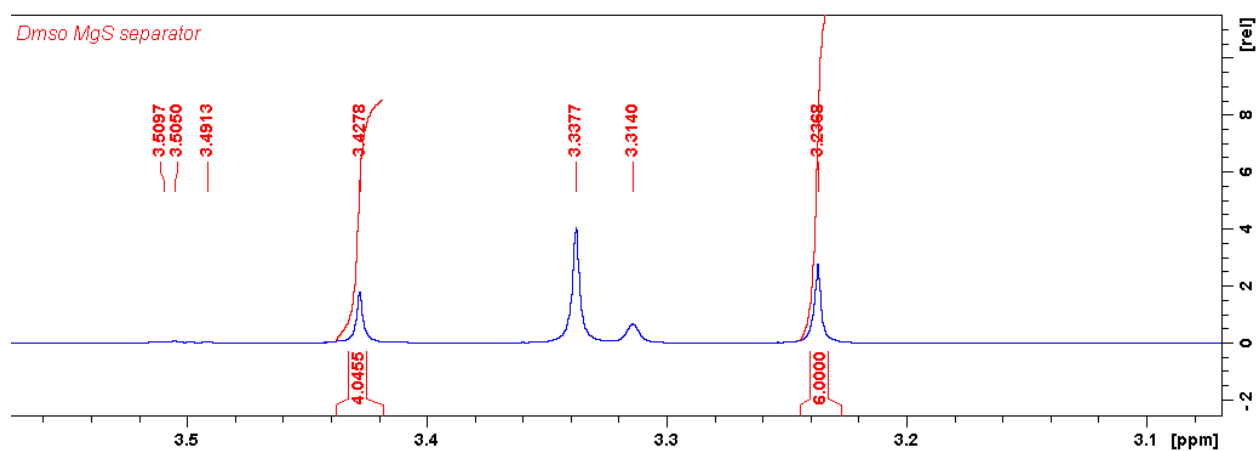


Figure S16B. ^1H NMR results for the DMSO dissolved Mg_xS_y sample alternate zoom to highlight DME peaks.

Further electrochemical data – discharge potential curves and EIS

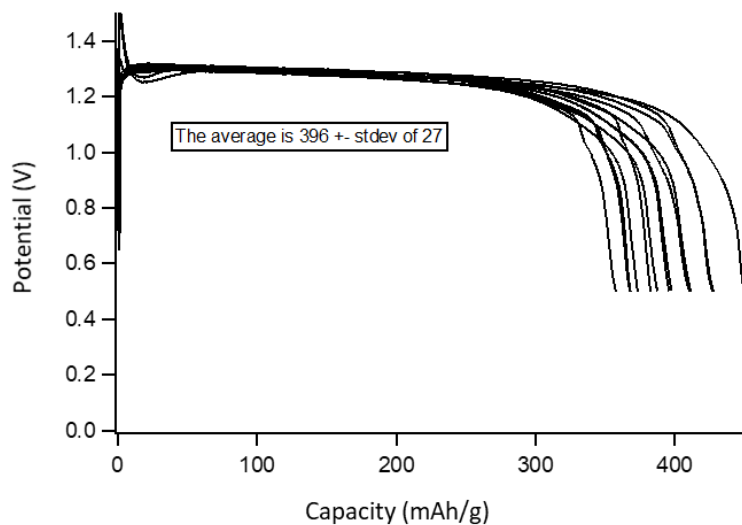


Figure S17. Discharge profiles of all cells used in this study that used 0.25 M MgTFSI₂ + 0.5 M MgCl₂ in DME, that were discharged to a cutoff potential of 0.5 V. The average capacity, 396 mAh/g, was used to calculate SOC for all cells in the manuscript, where 50% SOC = 200 mAh/g, etc. The plateau voltage is highly consistent, while the capacity varies slightly cell to cell.

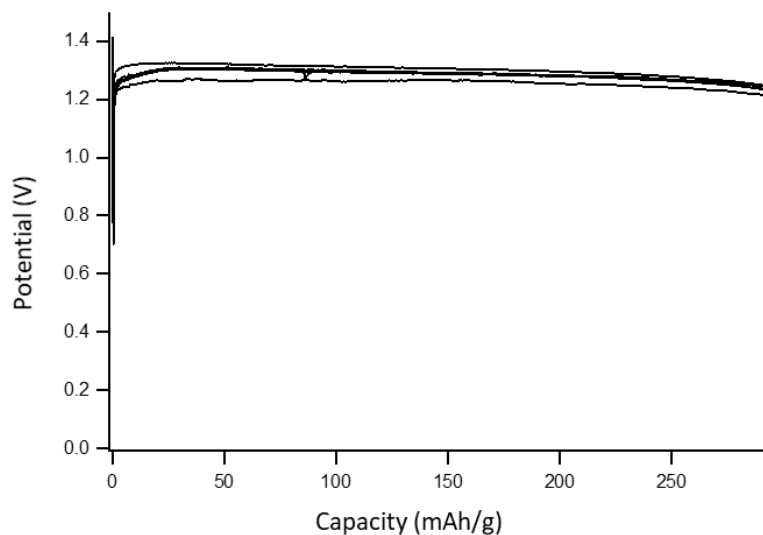


Figure S18. Discharge profiles of all cells used in this study that used 0.25 M MgTFSI₂ + 0.5 M MgCl₂ in DME, that were discharged to 300 mAh/g for use in the UPLC-MS experiment. The plateau voltage is highly consistent.

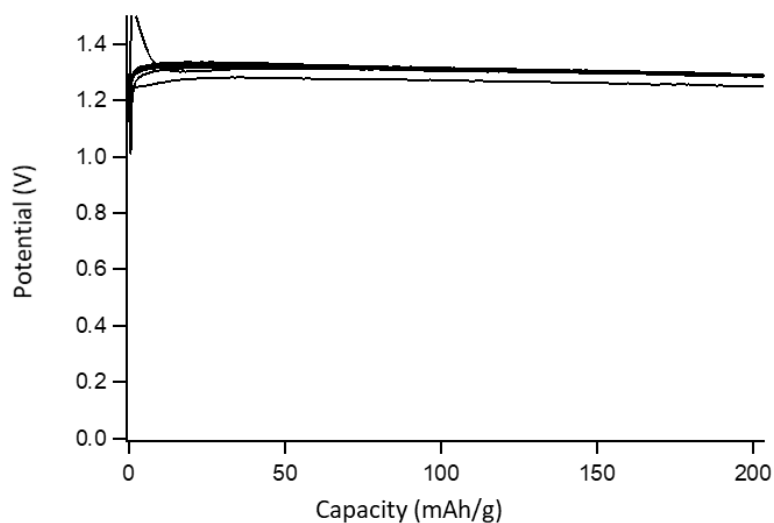


Figure S19. Discharge profiles of all cells used in this study that used 0.25 M MgTFSI₂ + 0.5 M MgCl₂ in DME, that were discharged to 200 mAh/g for use in the UPLC-MS experiment and UV/VIS experiment. The plateau voltage is highly consistent.

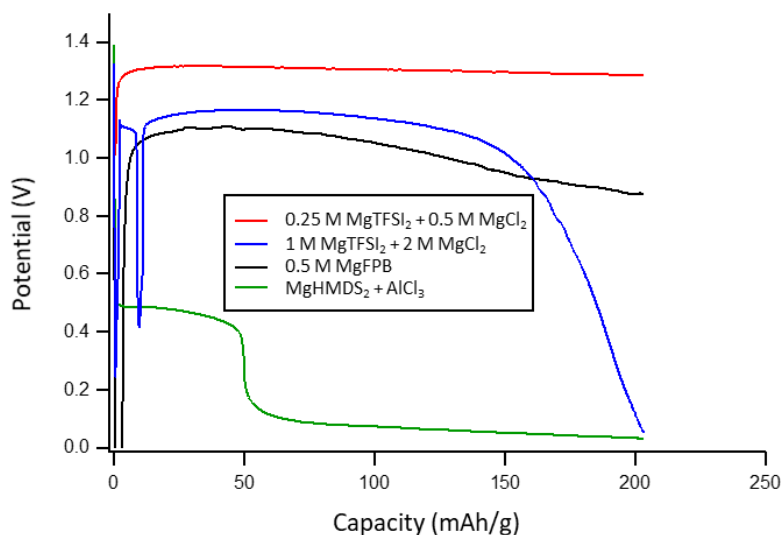


Figure S20. Representative discharge profiles for the different Mg electrolytes for cells discharged to 200 mAh/g at a rate of 0.1C.

Regarding the potential profiles in Figure S20, the wide variety of potentials for the sulfur reduction reaction are a result of the unique electrolyte chemistries. Each electrolyte, with different salts and solvents, has differing S₈ redox kinetics and different overpotentials on the Mg anode associated with Mg plating/dissolution, hence different performance. This is observed throughout the magnesium-sulfur literature.^{1,6-8}

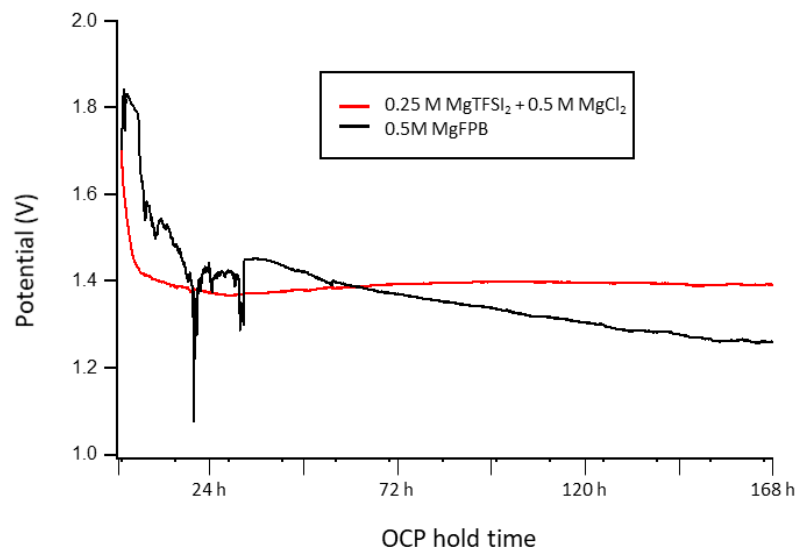


Figure S21. Open circuit potential of Mg-S cells held for 168 h prior to discharge.

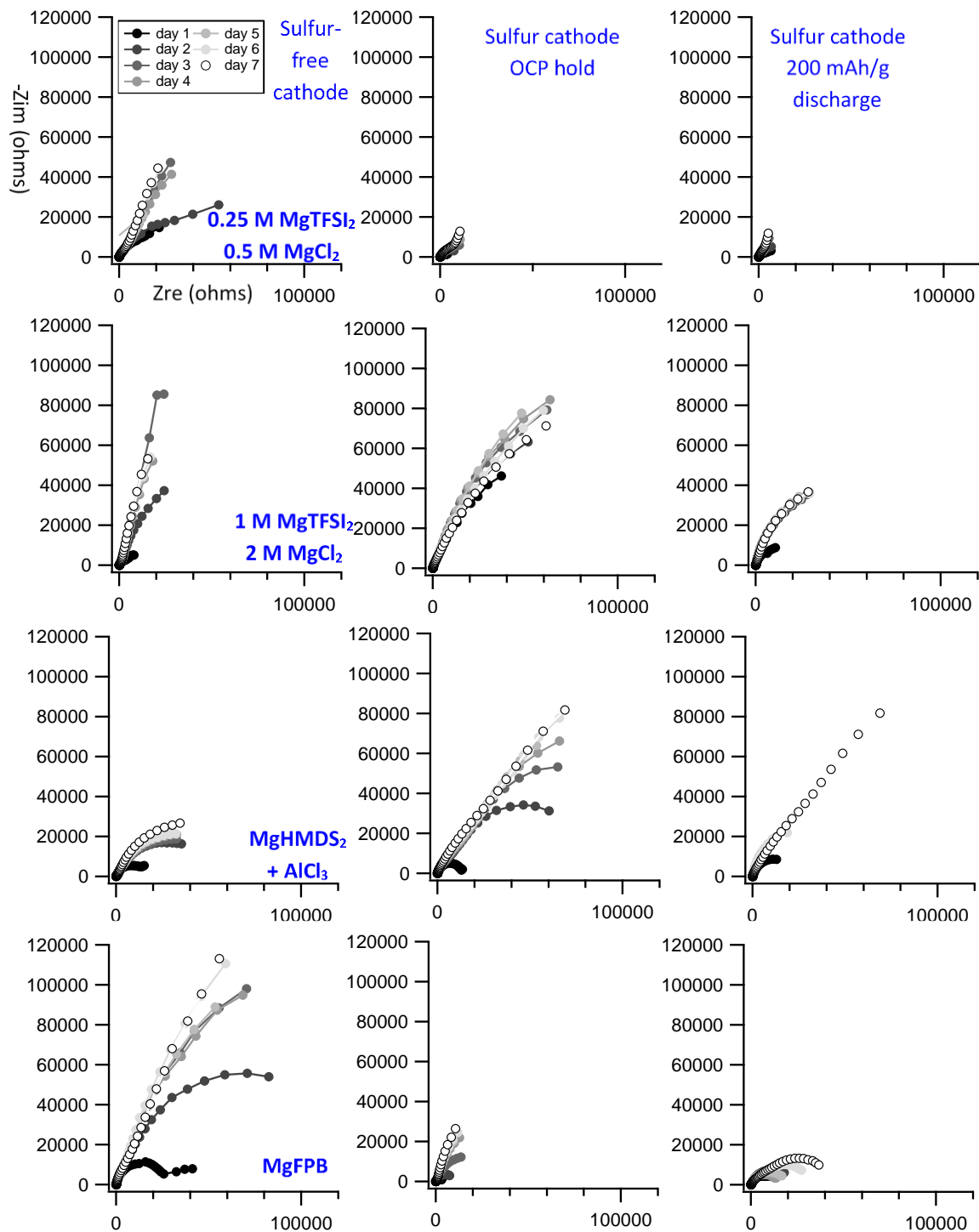


Figure S22 A. Electrochemical impedance spectroscopy results as a function of cell age for studied electrolytes for three cell types: sulfur-free cathode, sulfur cathode undischarged, sulfur cathode 200 mAh/g discharge. All shown on same impedance scale with XY parity.

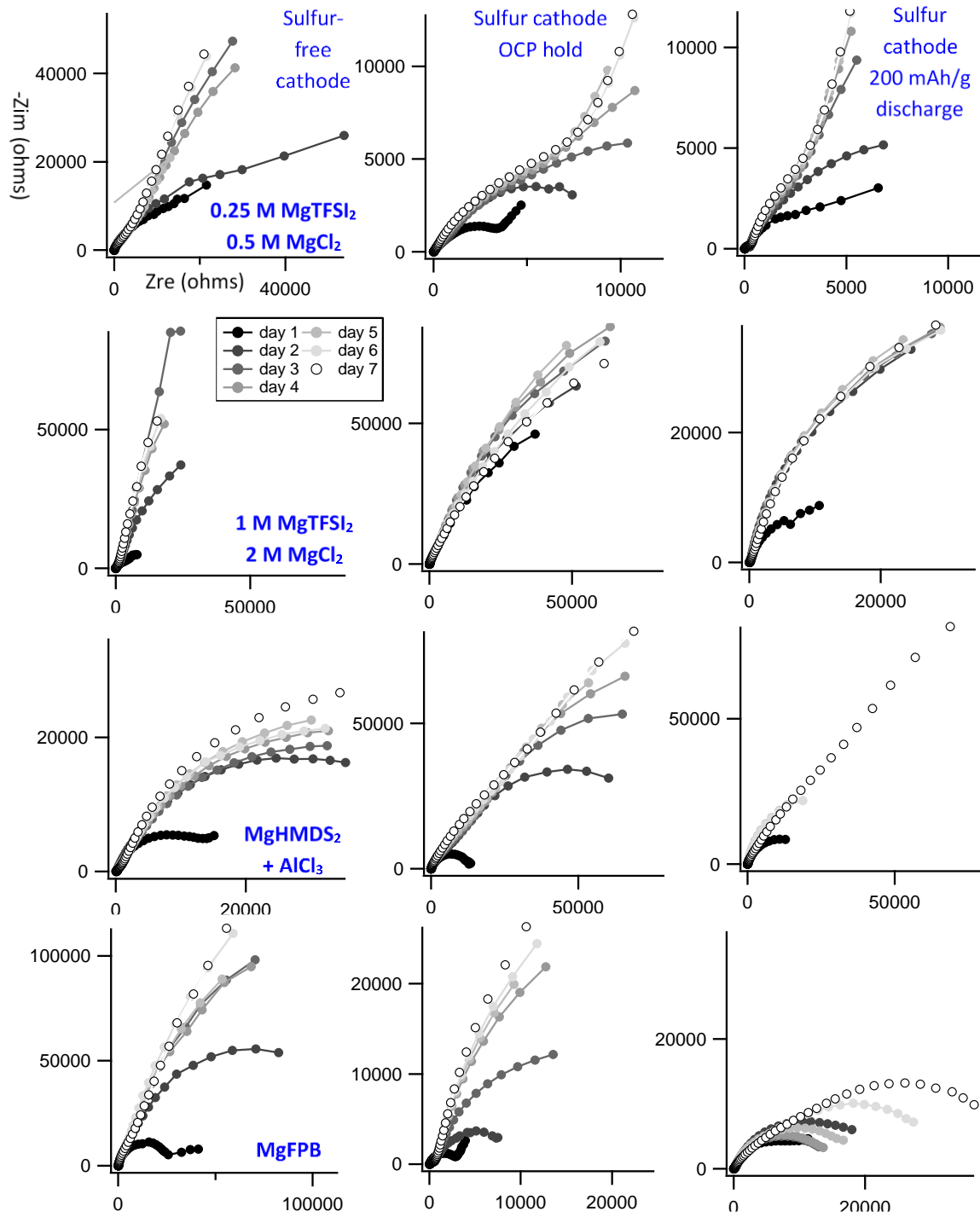


Figure S22 B. Same data as Figure S22A, but different scale to show nuance of each spectrum, with XY parity.

Regarding the EIS data in Figures S22A and S22B, our results are in qualitative agreement with those demonstrated by Häcker et al. in that for all cells, as time progresses the overall impedance increases.⁹ For each electrolyte, we studied three configurations: case 1 (left column) is for cells with a sulfur-free cathode, case 2 (middle column) is for cells with a sulfur cathode that was never discharged, case 3 (right column) is for cells with a sulfur cathode that was discharged 200 mAh/g. Speaking generally, for each electrolyte the formation of an absorption layer is evident from the increase of impedance in the case 1 cells. This result is consistent with previously observed phenomenon in Mg electrolytes, a characteristic that is largely unique to magnesium chemistry and can dominate the cell impedance.^{9,10}

In some scenarios, such as the case 2 and 3 cells for the MgFPB, 0.25 M MgTFSI₂ + 0.5 M MgCl₂, and the case 3 for the 1 M MgTFSI₂ + 2 M MgCl₂ cell, the formation of this absorption layer seems partially or fully suppressed. This would suggest the presence of sulfur/polysulfides, whether on the surface of the magnesium or in solution, prevent the formation of the high impedance absorption layer. Notably, however, the impedance increases with time for these cells as well, which would suggest the continued reaction of sulfur/polysulfides with the anode surface, resulting in the formation of a high-impedance SEI layer.

Disentangling the contribution of the absorption layer, the SEI formation, and contribution of the various cell components (both electrodes, electrolyte, etc.) to the impedance is outside the scope of this work in terms of the conclusions put forward. Therefore, we do not attempt to provide quantitative analysis of the EIS data nor do we over-interpret it.

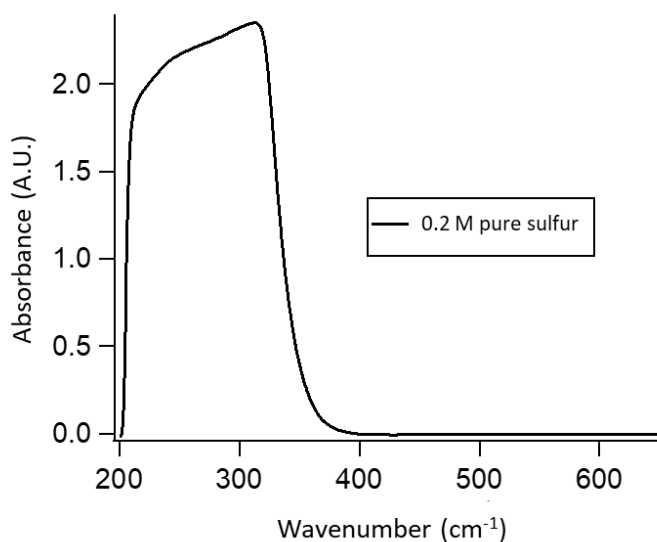


Figure S23. UV/VIS absorbance of a 0.2 M solution of S₈ dissolved in sieves-dried THF (reference = pure THF).

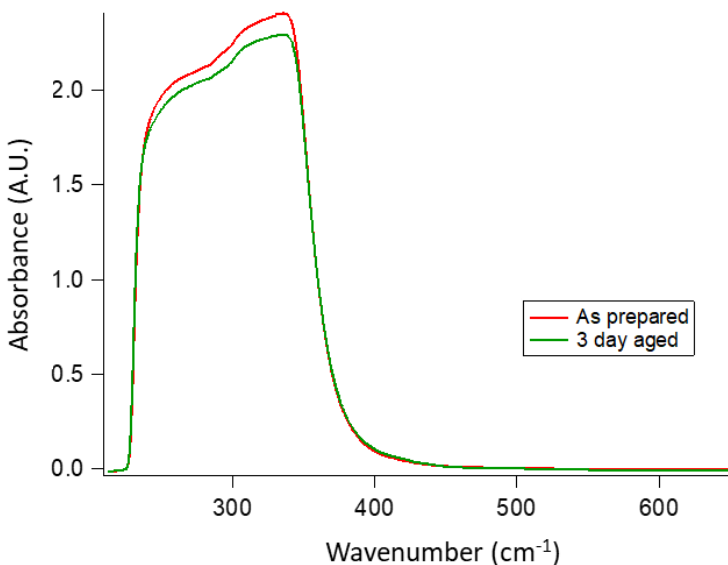


Figure S24. UV-VIS absorbance for magnesium polysulfides synthesized in the MgHMDS₂ + AlCl₃ in THF electrolyte. Reference = pristine electrolyte.

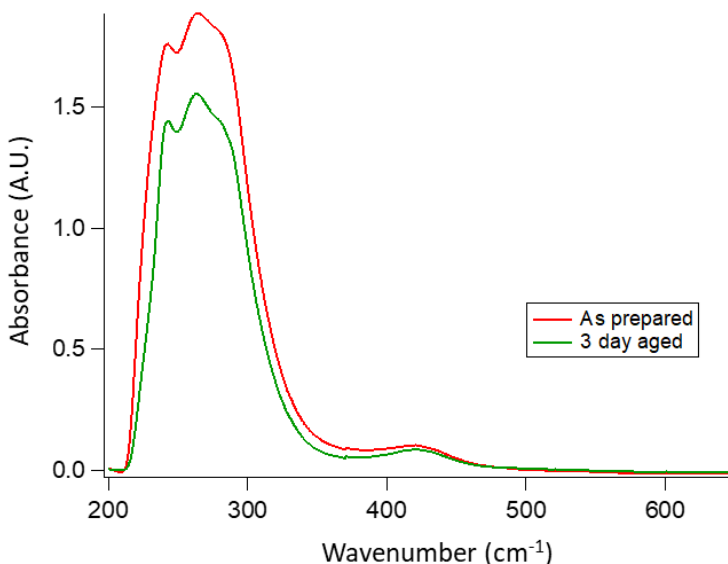


Figure S25. UV-VIS absorbance for magnesium polysulfides synthesized in the MgFPB in electrolyte. Reference = pristine electrolyte.

The solution of synthesized Mg-PS shown in the main text Figure 4A also contains dissolved, unreacted S₈. The presence of the polysulfides and the elevated synthesis temperature increases the solubility of S₈ (even after cooling), which is why S₈ is seen in the spectrum. The background subtraction used for Figure 4A is just the electrolyte (0.25 M MgTFSI₂ + 0.5 M MgCl₂ in DME) which contains no S₈. Figure S23 shows the absorbance pattern of pure S₈ dissolved in THF. Some of the absorbance bands (220 cm⁻¹, 250 cm⁻¹, 320 cm⁻¹) are not unique to S₈, they are also exhibited by polysulfides. The unique feature of S₈ is the

“blockiness” of the spectra, for lack of a better word, i.e. how it absorbs strongly and almost uniformly over the whole 200–320 cm^{-1} range. This peak characteristic is visible in Figure 4A because the S_8 contribution is not subtracted from Figure 4A. This feature is not visible in Figure 4B, C, and S because the S_8 is effectively subtracted because of how those background solutions were made. The peak at 380 cm^{-1} , observed in Figure 4A, is well described as S_4^{-2} by the literature, demonstrating these solutions do indeed contain synthesized Mg-PS.^{4,11} The synthesis of the Mg-PS is further validated using the UPLC-MS method described in the main text, with the results shown in Figure S36.

Figures S24 and S25 are the UV/VIS spectra of chemically synthesized magnesium polysulfides in the $\text{MgHMDS}_2 + \text{AlCl}_3$ and MgFPB electrolytes, respectively. This is the same experiment as the results shown in Figure 4A, which is for the 0.25 M $\text{MgTFSI}_2 + 0.5$ M MgCl_2 electrolyte. The absorbance in both of these solutions decreases with time, however there is the same degree of decrease for all absorbance bands. This is in contrast to the result of Figure 4A, where a decrease in one particular absorbance band is observed. The decrease in one absorbance band is attributed to the decrease in concentration of a certain polysulfide. The equal decrease in absorbance bands in the MgHMDS and MgFPB cases may indicate either all the polysulfides in these solutions are decreasing in concentration, or that there is a decrease in elemental sulfur S_8 concentration. Given the “blocky” nature of absorbance of S_8 seen in Figure S23, a uniform decrease in absorbance in S24 and S25 could be explained by decreased S_8 concentration. Indeed, the MgFPB solution shows a very minor amount of visible precipitate at the end of 72 h, however the MgHMDS does not.

It is worth noting that, in order for magnesium polysulfides to be synthesized in ethereal solvents, the presence of magnesium salts seems necessary. Attempts to synthesize magnesium polysulfides in ethers without the presence of a Mg salt have been unsuccessful. Again, the fact that these syntheses are successful indicates that there is a non-faradaic conversion of S_8 to ionic magnesium polysulfide taking place in these electrolytes.

Table S3. Solubility of sulfur in various systems relevant to this work. * denotes dried below 10 ppm water.

System	S8 Solubility	Reference
Tetrahydrofuran (THF)*	0.50 M	This work
Dimethoxyethane (DME)*	0.068 M	This work
Diglyme (DEG)*	0.12 M	This work
0.25 M $\text{MgTFSI}_2 + 0.5$ M MgCl_2 electrolyte (DME)	0.071 M	¹
1 M $\text{MgTFSI}_2 + 2$ M MgCl_2 electrolyte (DME)	0.0096 M	¹
$\text{MgHMDS}_2 + \text{AlCl}_3$ electrolyte (THF)	0.25 M	This work
MgFPB electrolyte (DEG)	0.029 M	This work

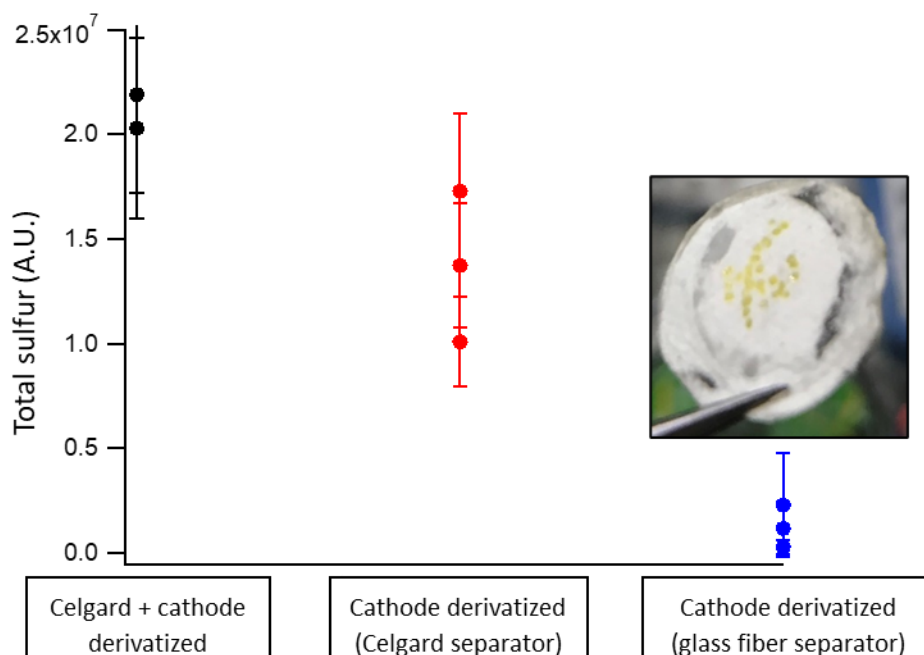


Figure S26. Total solid ionic sulfur quantified by UPLC-MS method for different cell components, either both the separator and cathode or just the cathode. Cells are full Mg-S cells using the 0.25 M MgTFSI₂ + 0.5 M MgCl₂ in DME electrolyte discharged to 0.5 V (396 mAh/g on average). Inset photo shows a glass fiber separator recovered from a discharged cell.

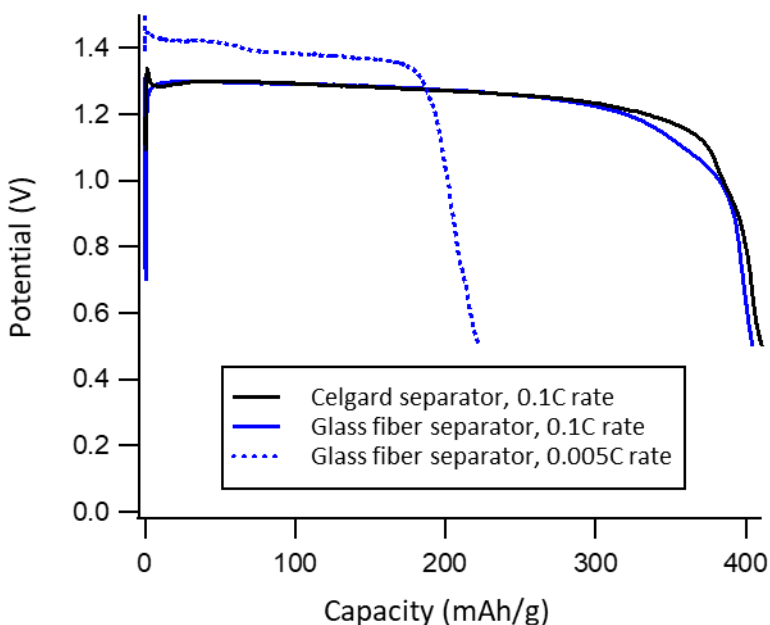


Figure S27. 1st cycle discharge profiles for various Mg-S cells using the 0.25 M MgTFSI₂ + 0.5 M MgCl₂ in DME electrolyte.

Figures S26 and S27 demonstrate that the chemical precipitation of polysulfides, the second aspect of self-discharge, happens on time-scales relevant to active cell discharge. Figure S26 shows that the

amount of solid ionic sulfur in *the cathode* measured by the UPLC-MS method differs depending on what separator is used. In the case of cells using Celgard, roughly half of the solid (poly)sulfides precipitate on the cathode, and half in the Celgard separator. In the case of cells that use glass fiber, the amount of solids detected on the cathode is greatly decreased, implying large precipitation within the separator. These deposits are in fact seen easily in the inset photo shown in the inset of Figure S26. However, because the potential profiles of the cells using the two types of separators are nearly identical at 0.1C (Figure S27), in both cases the same amount of sulfur is electrochemically accessed.

So why does one case result in a large amount of solid sulfur precipitates on the cathode, while the other does not? The two separators are quite different in size and porosity (Celgard is 25 μm thick and microporous, glass fiber is 200 μm thick and macroporous) meaning the proportion of electrolyte absorbed by each separator is different. As both cells use 160 μL of electrolyte, the higher volume glass fiber separator will absorb more of the electrolyte, meaning there is less in direct contact with the cathode.

Combining the facts that the spatial location of the (poly)sulfide deposits can be changed by changing the electrolyte distribution in the cell (i.e. changing the separator), and that changing this distribution does not impact the electrochemical capacity delivered by the cell, a major amount of the solid ionic (poly)sulfides formed as the cell discharges comes not from electrochemical reduction, but from the chemical precipitation process. The chemical precipitation process results in a major non-faradaic loss of active material as the cell discharges. Even when the precipitation happens in the cathode region and not in the separator, the precipitates do not have good electronic contact and therefore are electronically inaccessible.

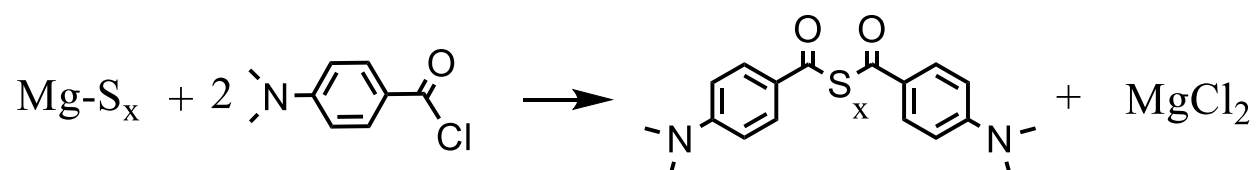
The cells that are run at 0.1C take just over 2 h to fully discharge to 0.5 V, which means the kinetics of the precipitation process must be fast. This is even more evident given that the precipitation process is not yet highly active when the cell has been discharged to 200 mAh/g (half-way) as seen in Figure 3. Likely, once the average chain length of polysulfides in solution is sufficiently lowered (by combination of non-faradaic reduction at the anode and faradaic reduction at the cathode), the precipitation process ensues rapidly. In theory, then, if the cell is discharged faster, more sulfur should be accessible electrochemically before it precipitates. Conversely, if the cell is discharged more slowly, more sulfur is lost due to chemical precipitation and the discharge capacity will be lowered. This is exactly the case, as can be seen in the 0.005C rate cell shown in Figure S27. In this cell, the discharge is so slow that essentially only the capacity associated with converting covalent S_8 to S_8^{2-} is accessed; all the produced S_8^{2-} diffuses from the cathode where it can be reduced via the non-faradaic process at the anode until it precipitates, rendering it inaccessible.

These results drive home the importance of considering the precipitation aspect of the self-discharge pathway. Without addressing this phenomenon, after one cycle most of the cell active material will be lost. Future work should involve looking at published Mg-S literature that demonstrates good capacity retention with cycling, and interpreting those results within this framework and specifically asking the question: what about the cell design, electrolyte, cathode, etc. prevents the loss of active material via

the precipitation route? An answer to this question will point the way towards highly reversible, and therefore practical, Mg-S batteries.

Further discussion of the UPLC-MS – Method development

This section contains a more detailed description of the UPLC-MS technique. The chemistry of functionalization is presented in Scheme S1. Ionic polysulfides are converted to organic polysulfides, which due to the dimethylamino aromatic components have good affinity with the UPLC column. This allows for the separation of the organic polysulfides on the basis of molecular weight, with a logarithmic relationship between retention time and number of sulfur atoms in the compound.¹² Clear separation of the compounds on the basis of the number of sulfur atoms they contain allows for accurate quantification of each compound.



Scheme S1. Derivatization reaction of magnesium polysulfides.

A representative chromatogram is presented below in Figure S28. The logarithmic relationship between the number of sulfur atoms per each compound and retention time is clearly present. The total sulfur content of the cell is found by integrating the area under the appropriate peaks (denoted with *), multiplying by the number of sulfur atoms in that specific compound, and summing the results.

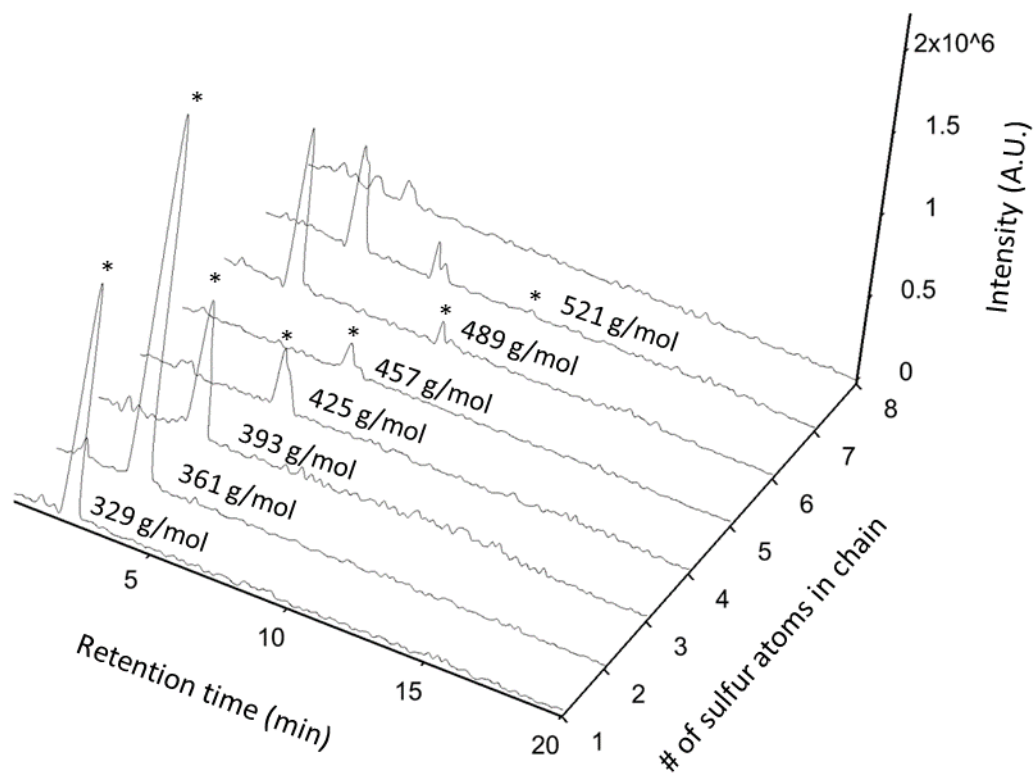


Figure S28. Mass specific chromatograms of a derivatized Mg-S cell (200 mAh/g discharged, no rest, sample #1). Peaks corresponding to the derivatized compounds marked with *.

The peaks are correctly identified as the proposed compound on the basis of isotope pattern, an example of which is shown in Figure S29 for D-S1-D-H+ (329 g/mol). By the same approach, the peaks at 2.47 min in the S6 chromatogram and at 3.2 min and 6.2 min in the S7 chromatogram (and any other peaks in a chromatogram) are shown not to be derivatized polysulfides. If the isotope pattern does not match the expected organic polysulfide pattern, the peak is not included in the calculation of total sulfur. The raw chromatograms for all the data shown in the main text Figure 3 and Figure S26 are presented at the end of the supporting information in **Appendix 1**.

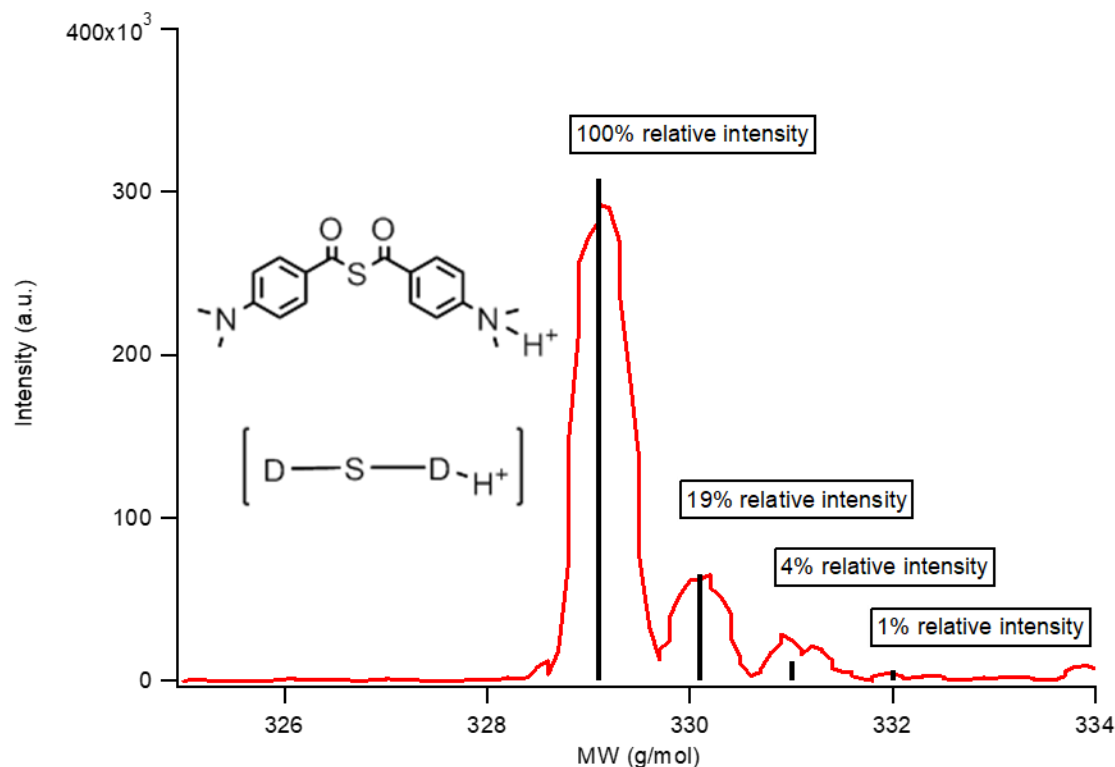


Figure S29. Mass spectrum for 329 g/mol, D-S-D-H⁺ (red), with calculated isotope pattern (black bars).

This technique has previously been used to determine the speciation of polysulfides in Li-S batteries at a given state of discharge.¹² In attempting to reproduce this experiment, we found that our mass spectrometry results did not reflect the actual cell polysulfide chain length distribution. The experimental procedure reported in the above reference was repeated as faithfully as possible, and when that did not reproduce the expected results, the parameters of the technique were systematically varied. We found that our results were sensitive to experimental parameters such as the amount of derivatizing agent used in the work-up, selection of the mobile phase, column, and sample dilution/preparation. Unfortunately, no combination of parameters yielded believable results for the polysulfide speciation within the cell.

This result, that the speciation observed with the UPLC-MS does not reflect the cell speciation, is realized in numerous ways. First, the amount of derivatizing agent used changes the observed organic polysulfide speciation chain length. Second, the chain length speciation observed for a partially discharged Li-S cell does not match with the known polysulfide speciation for Li-S cells at this stage of discharge. Third, higher order (S₉+) organic polysulfides are observed in cases with high initial ionic polysulfide concentration. Finally, the detected amount of a compound of a given chain length has a logarithmic relationship to the number of S atoms in the compound. These points are explored in detail in the following section.

Effect of derivatizer amount and Li-S mismatch

Two identical Li-S cells, the discharge profiles of which are presented in Figure S30, were discharged to 2.2 V. Each cell was then derivatized with a procedure similar to that of the Mg-S cells, except the first Li-S cell was treated with 1.5 mg of derivatizing agent and the second cell with 2.0 mg of derivatizing agent. The full chromatogram of these two samples is presented in Figure S31.

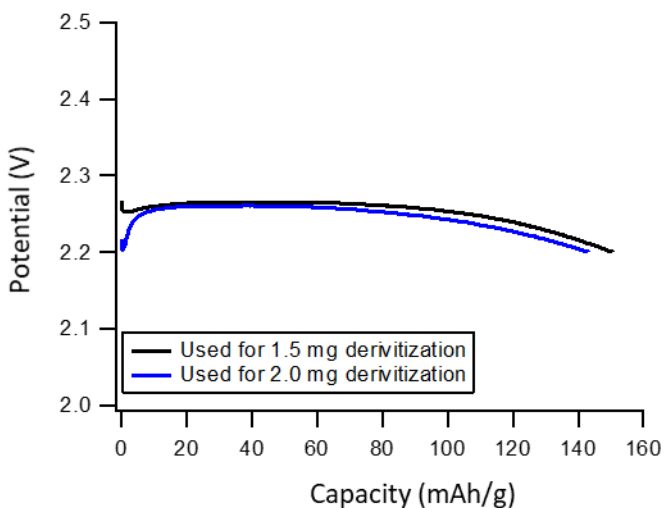


Figure S30. Li-S cells discharged to 2.2 V for MS derivitization.

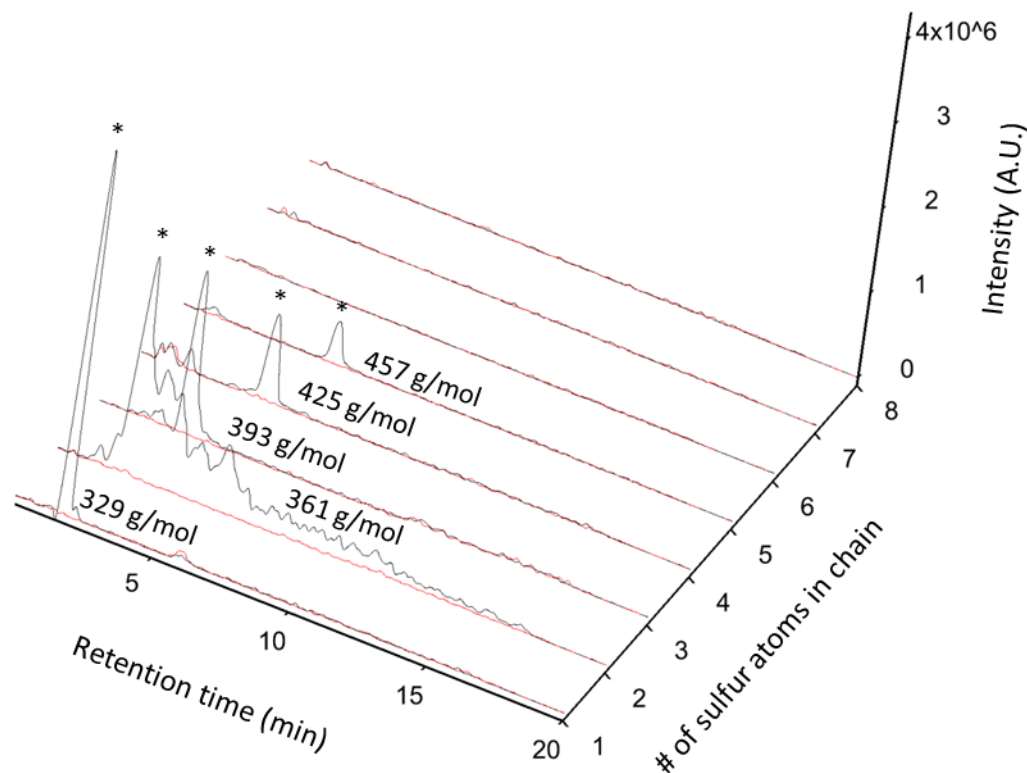


Figure S31. Mass specific chromatogram of derivatized Li-S cells, prepared with different amounts of derivatizing agent. **Red chromatogram** = cell prepared with 1.5 mg derivatizing agent. **Black chromatogram** = cell prepared with 2.0 mg derivatizing agent. Peaks corresponding to the derivatized compounds marked with *.

Immediately apparent is the impact of derivatizer amount on the mass spectrometry results, in that 1.5 mg do not appear to be enough to produce any D-S_x-D species. Perhaps, the first functionalization of an ionic polysulfide is more favorable than the second functionalization, and if 1.5 mg are not enough to functionalize every species at least once, then no D-S_x-D compounds would be observed in the chromatogram. At any rate, the apparent sensitivity of the experiment to derivatizer amount led to the standard use of 5 mg of derivatizer for each Mg-S sample. If the sensitivity of the MS results to the derivatizer amount used was not enough to call into question the accuracy of polysulfide speciation, then the speciation observed in the 2.0 mg Li-S cell can leave no doubt. The speciation observed in the chromatogram indicates a high concentration of monosulfide, disulfide, and short chain polysulfides. A Li-S cell typically exhibits two distinct discharge plateaus, one from about 2.5 V to 2 V, and another from about 1.9 V to 1.7 V. When the cell is still in the first plateau stage, it is well known that the lithium polysulfide speciation consists of long-chain polysulfides.¹³ If the results of the 2.0 mg Li-S MS cell were representative of the true cell speciation, the observed species would be D-S_x-D for x = 8, 7, 6, 5, as opposed to the short chain species that were observed.

Higher order (S₉₊) organic polysulfides: In some cases, the formation of higher order organic polysulfides S₉, S₁₀, and S₁₁ were observed. An example is visible in Figure A8. This speciation is impossible to form electrochemically when starting from covalent S₈, further indicating that the

derivatization process alters the polysulfide speciation. The higher order organic sulfides were only observed in samples that had displayed high concentrations of ionic sulfur. In general, S9 is only observed if S8 was present, S8 only if S7 was present, and so on. The derivatization procedure appears to bias the formation of S1 first, forming higher order species as the initial ionic polysulfide concentration increases. The reason for this is unknown, but may stem from decreased stability of the higher order compounds. If more sulfur is initially present, the activity of sulfur atoms in solution are increased, which may help stabilize the higher order polysulfides. This is related to the final point.

Logarithmic dependence of compound concentration on sulfur atom chain length: Figure S32 shows the roughly logarithmic dependence of the amount of a given organic polysulfide on the number of sulfur atoms it contains. This relationship is most strongly observed for samples with high initial concentrations of ionic polysulfides. This relationship points to the speciation being governed by processes that influence the derivatization reaction, such as compound solubility, sulfur activity, etc. as opposed to the true cell speciation. Alternatively, this result could be a reflection of technique bias; larger compounds may decompose or get stuck on the UPLC column or have decreased solubility in the mobile phase.

Given these reasons, the polysulfide speciation observed is assumed not to be representative of the cell speciation. However, even though the true cell speciation cannot be obtained with this mass spectrometry method, the relative number of sulfur atoms in the form of ionic poly(sulfides) in a cell can be conclusively determined. It is on this basis that the self-discharge process of Mg-S batteries is investigated.

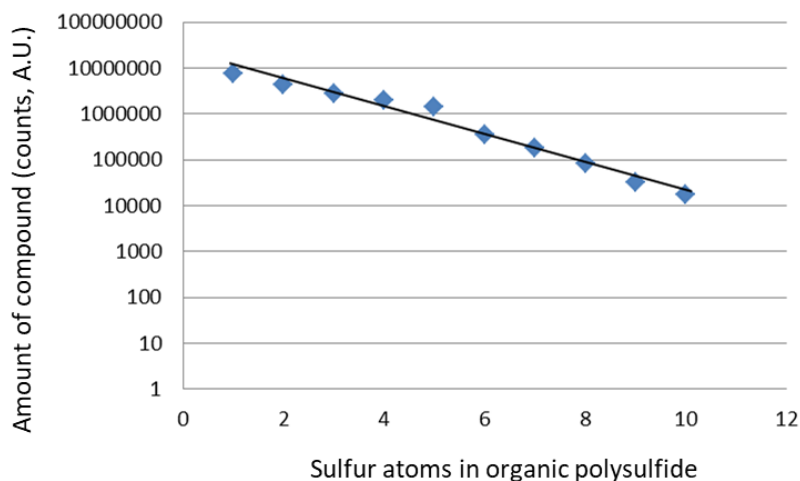


Figure S32. Amount of organic polysulfide compound D-S_x-D detected as function of number of sulfur atoms X for a sample with high initial ionic polysulfide concentration (200 mAh/g discharged, 168 h aged 0.25 M MgTFSI₂ + 0.5 M MgCl₂ in DME cell).

Further verification of UPLC-MS method applied to Mg-S chemistry

Derivatization of solid Mg_xS_y

Figure S33 demonstrates proof that the derivatization reaction successfully reacts with the solid poly(sulfide) species observed as precipitation on the cell separators and cathode. In the upper left photograph, yellow solid deposits are visible on the separator even after the separator has been washed with DME. In the upper right photograph, the separator has been placed in a solution containing DME with derivatizing agent DBC. The previously solid precipitates can be seen reacting and dissolving, evidenced by the spread of yellow across the separator. In the bottom photograph, the separator was removed from the solution and dried *without any further rinsing*, revealing the now pristine separator and clear yellow solution of organic polysulfides.



Figure S33. Dissolution of solid magnesium (poly)sulfide species via reaction with derivatizer. Upper left, separator with deposits circled. Top right, separator in solution of derivatizing agent + DME. Bottom, dried separator after removing from solution and yellow derivatized polysulfides.

Identifying the first step in the Mg-S self-discharge

In one of the three literature studies that had previously observed Mg-S self-discharge, the first step of the process, conversion of S_8 to S_8^{2-} , was proposed to be a result of S_8 reacting with the electrolyte.¹⁴ In the other studies, the first step was proposed to be a result of S_8 directly reacting with Mg metal.^{9,15} With use of the UPLC-MS technique, we are able to definitively establish that Mg metal must be present for the self-discharge process to begin.

Two samples were prepared and run on the UPLC-MS. The first sample consisted of 0.76 mg of sulfur powder stirred into 160 μ L of 0.25 M $MgTFSI_2$ + 0.5 M $MgCl_2$ in DME. This solution was stirred for an hour, then transferred to a solution of 5 mg derivatizing agent (DBC) suspended in 100 μ L of DME. The

solution was then processed per the standard UPLC-MS workup outlined in the experimental section. The chromatogram for this sample is shown in Figure S34.

The second sample was prepared from a Mg-S cell that had not been discharged. Just as described in the experimental for all of the Mg-S cells, this cell consisted of a cathode containing 0.76 mg sulfur, 160 μL of 0.25 M MgTFSI_2 + 0.5 M MgCl_2 in DME, a Celgard separator, and a Mg anode. This cell was assembled, rested at OCP for 1 h, then disassembled and processed per the standard technique. The chromatogram for this sample is shown in Figure S35.

Considering Figures S34 and S35, both samples contain a low concentration of analyte compared to the innate noise of the technique. When there were peaks that matched the known retention times for the derivatized organic sulfides of various chain lengths, the peak is highlighted with red to make it easier to see. Unfortunately, in both cases the concentration is so low that there is not a strong enough signal to definitively identify the analyte on the basis of isotope pattern. On the basis of retention time, the peaks are assumed to be the derivatized compounds. Comparing the relative intensities, it is clear that a much lower, essentially negligible, amount of ionic polysulfides are formed when the sulfur powder is stirred with the electrolyte and derivatizer. By contrast, in the sample where Mg metal is present, the logarithmic sulfur atom : retention time relationship is observed for peaks with non-negligible peak area. This result demonstrates that Mg metal is reacting with solubilized S_8 and converting it into S_8^{2-} in a non-faradaic self-discharge process, in as little time as 1 hour.

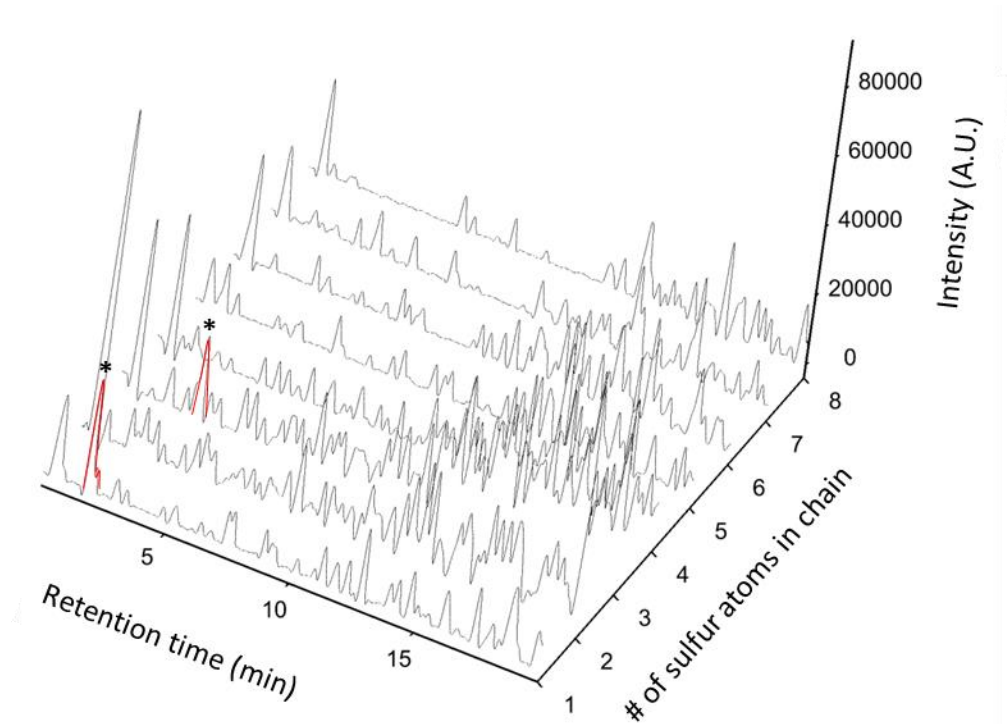


Figure S34. Mass specific chromatogram for sample of sulfur powder + electrolyte. Peaks corresponding to the derivatized compounds marked with * based on retention times from other chromatograms.

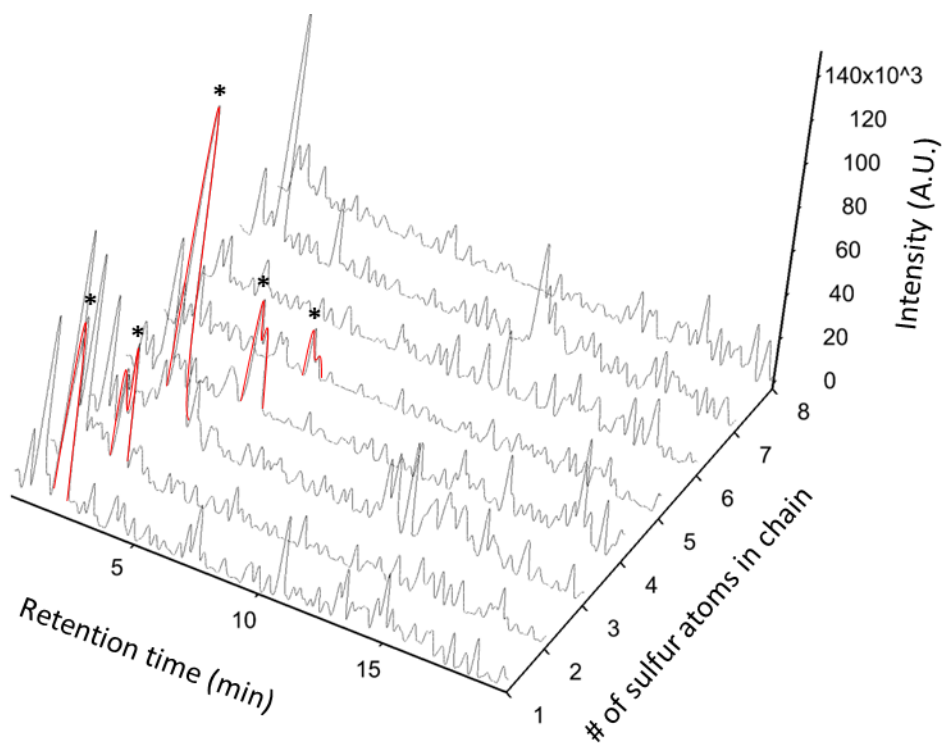


Figure S35. Mass specific chromatogram for sample harvested from full Mg-S cell held at OCP. Peaks corresponding to the derivatized compounds marked with *.

As one final demonstration, the synthesized solution of magnesium polysulfides (sulfur powder + of 0.25 M MgTFSI₂ + 0.5 M MgCl₂ in DME + magnesium powder) is derivatized and analyzed with UPLC-MS, which is shown in Figure S36. The presence of organic polysulfides in the chromatogram proves the synthesis of magnesium polysulfides is successful and that, once again, Mg metal is required for the spontaneous formation of ionic polysulfides. These peaks are definitively identified with isotope patterns. It should be noted that the MgTFSI₂ and MgCl₂ salts are also required for this direct synthesis to be successful.

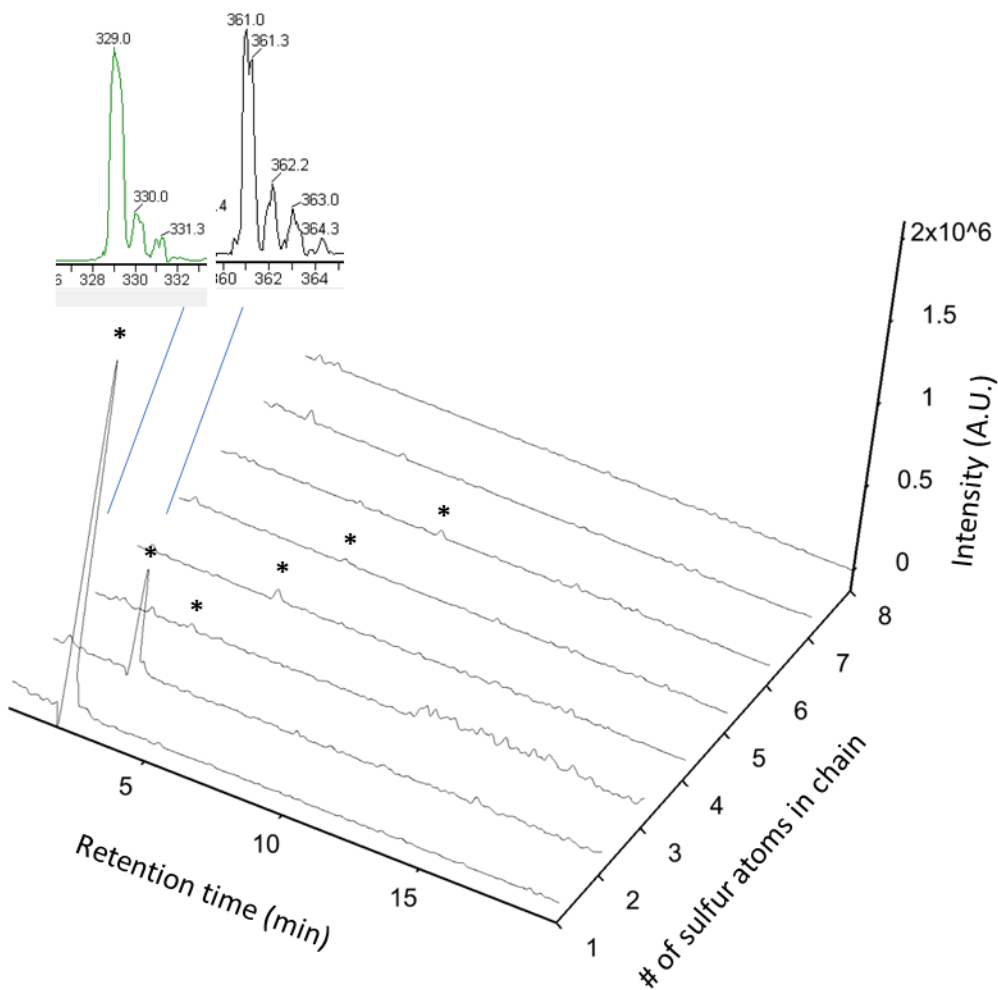


Figure S36. Chromatogram of derivatized solution of synthesized magnesium polysulfides (sulfur powder + of 0.25 M MgTFSI₂ + 0.5 M MgCl₂ in DME + magnesium powder). Peaks corresponding to the derivatized compounds marked with *. Inset shows isotope pattern of first two peaks.

References

- 1 T. Gao, S. Hou, F. Wang, Z. Ma, X. Li, K. Xu and C. Wang, *Angew. Chemie - Int. Ed.*, 2017, **56**, 13526–13530.
- 2 J. Luo, Y. Bi, L. Zhang, X. Zhang and T. L. Liu, *Angew. Chemie - Int. Ed.*, 2019, **58**, 6967–6971.
- 3 G. Bieker, J. Wellmann, M. Kolek, K. Jalkanen, M. Winter and P. Bieker, *Phys. Chem. Chem. Phys.*, 2017, **19**, 11152–11162.
- 4 G. Bieker, D. Diddens, M. Kolek, O. Borodin, M. Winter, P. Bieker and K. Jalkanen, *J. Phys. Chem. C*, 2018, **122**, 21770–21783.
- 5 G. R. Fulmer, A. J. M. Miller, N. H. Sherden, H. E. Gottlieb, A. Nudelman, B. M. Stoltz, J. E. Bercaw and K. I. Goldberg, *Organometallics*, 2010, **29**, 2176–2179.

- 6 A. Du, Z. Zhang, H. Qu, Z. Cui, L. Qiao, L. Wang, J. Chai, T. Lu, S. Dong, T. Dong, H. Xu, X. Zhou and G. Cui, *Energy Environ. Sci.*, 2017, **10**, 2616–2625.
- 7 Z. Zhang, Z. Cui, L. Qiao, J. Guan, H. Xu, X. Wang, P. Hu, H. Du, S. Li, X. Zhou, S. Dong, Z. Liu, G. Cui and L. Chen, *Adv. Energy Mater.*, 2017, **7**, 1602055.
- 8 W. Li, S. Cheng, J. Wang, Y. Qiu, Z. Zheng, H. Lin, S. Nanda, Q. Ma, Y. Xu, F. Ye, M. Liu, L. Zhou and Y. Zhang, *Angew. Chemie - Int. Ed.*, 2016, **55**, 6406–6410.
- 9 J. Häcker, C. Danner, B. Sievert, I. Biswas, Z. Zhao-Karger, N. Wagner and K. A. Friedrich, *Electrochim. Acta*, 2020, **338**, 135787.
- 10 O. Tutusaus, R. Mohtadi, N. Singh, T. S. Arthur and F. Mizuno, *ACS Energy Lett.*, 2017, **2**, 224–229.
- 11 M. Salama, R. Attias, B. Hirsch, R. Yemini, Y. Gofer, M. Noked and D. Aurbach, *ACS Appl. Mater. Interfaces*, 2018, **10**, 36910–36917.
- 12 D. Qu, D. Zheng, D. Qu, X. Q. Yang, X. Yu and H. S. Lee, *Adv. Energy Mater.*, 2015, **5**, 1401888.
- 13 A. Manthiram, Y. Fu and Y. S. Su, *Acc. Chem. Res.*, 2013, **46**, 1125–1134.
- 14 B. P. Vinayan, H. Euchner, Z. Zhao-Karger, M. A. Cambaz, Z. Li, T. Diemant, R. J. Behm, A. Gross and M. Fichtner, *J. Mater. Chem. A*, 2019, **7**, 25490–25502.
- 15 R. Richter, J. Häcker, Z. Zhao-Karger, T. Danner, N. Wagner, M. Fichtner, K. A. Friedrich and A. Latz, *ACS Appl. Energy Mater.*, 2020, **3**, 8457–8474.

Appendix 1. Raw mass spectrometry chromatograms for data points shown in Figure 3 in main text and Figure S35 in Supplementary Information. Peaks identified with both a retention time and area are verified to be D-S_x-D with isotope pattern, and used for calculation of the total ionic sulfur.

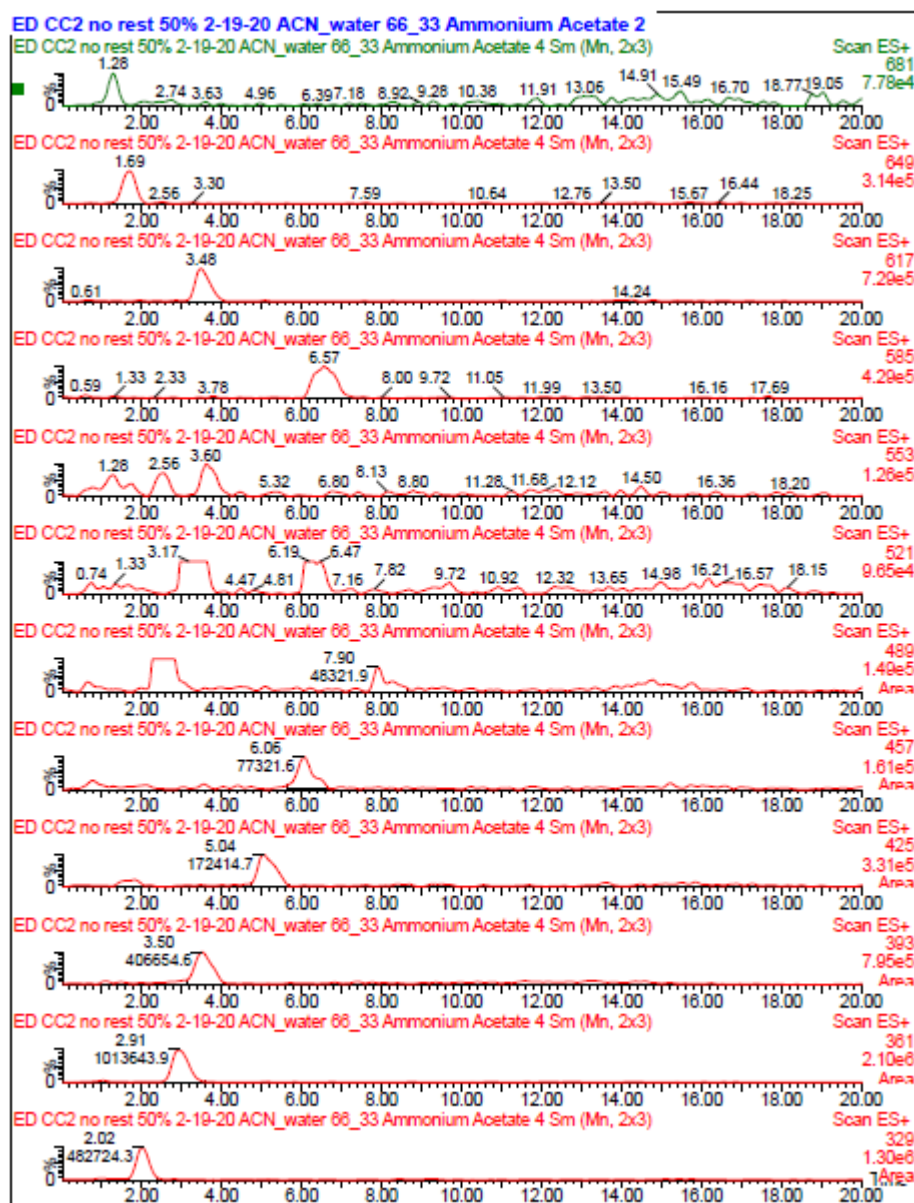


Figure A1. 200 mAh/g discharged, no rest, sample #1.

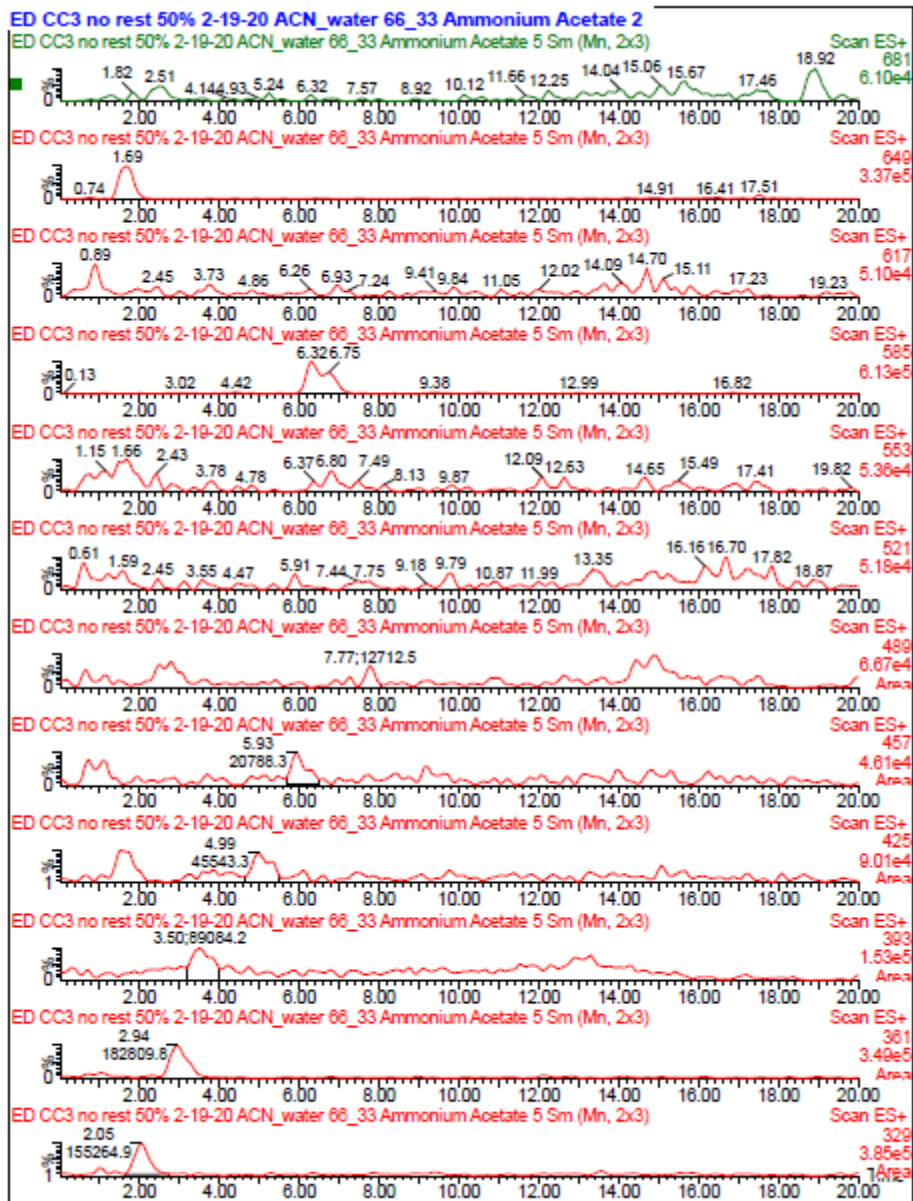


Figure A2. 200 mAh/g discharged, no rest, sample #2.



Figure A3. 200 mAh/g discharged, no rest, sample #3.

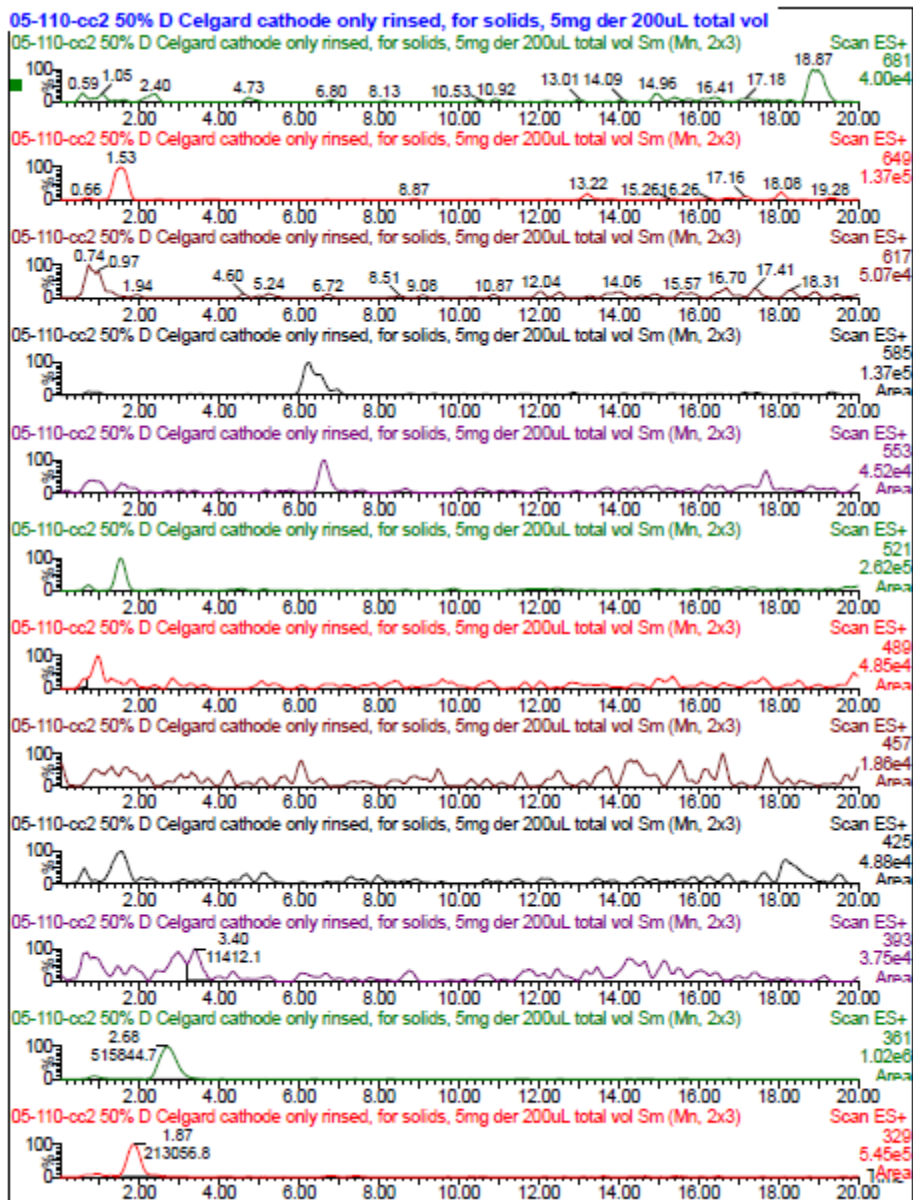


Figure A4. 200 mAh/g discharged, no rest, sample #4.

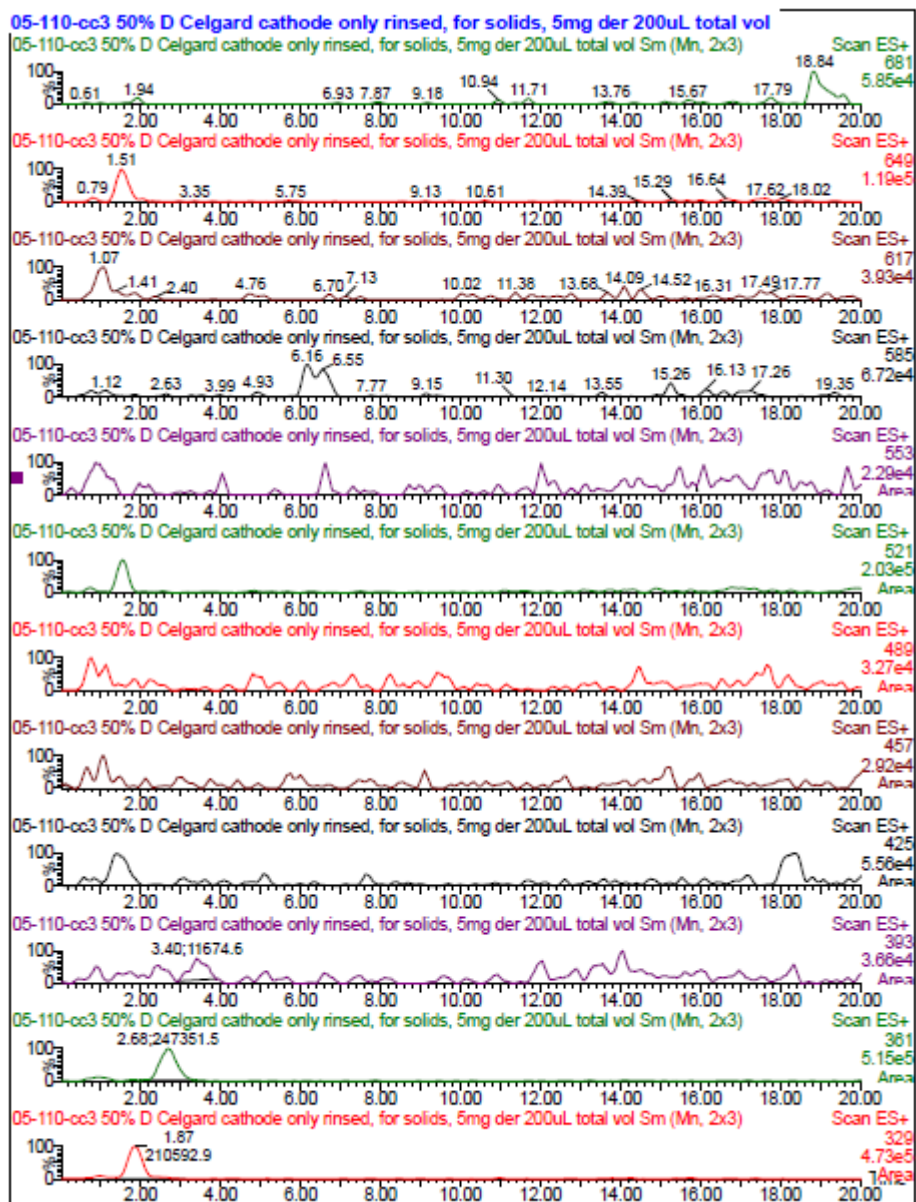


Figure A5. 200 mAh/g discharged, no rest, sample #5.

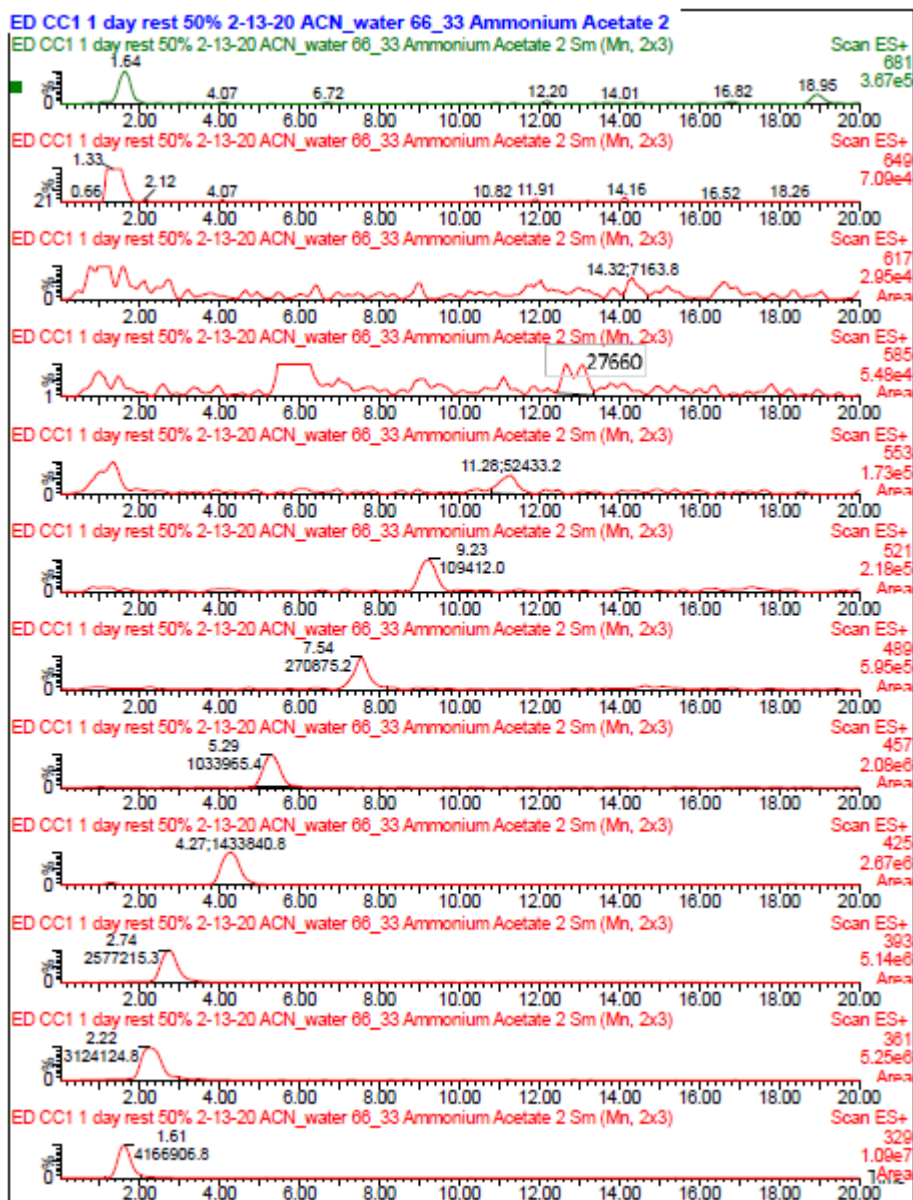


Figure A6. 200 mAh/g discharged, 24 h aged, sample #1.

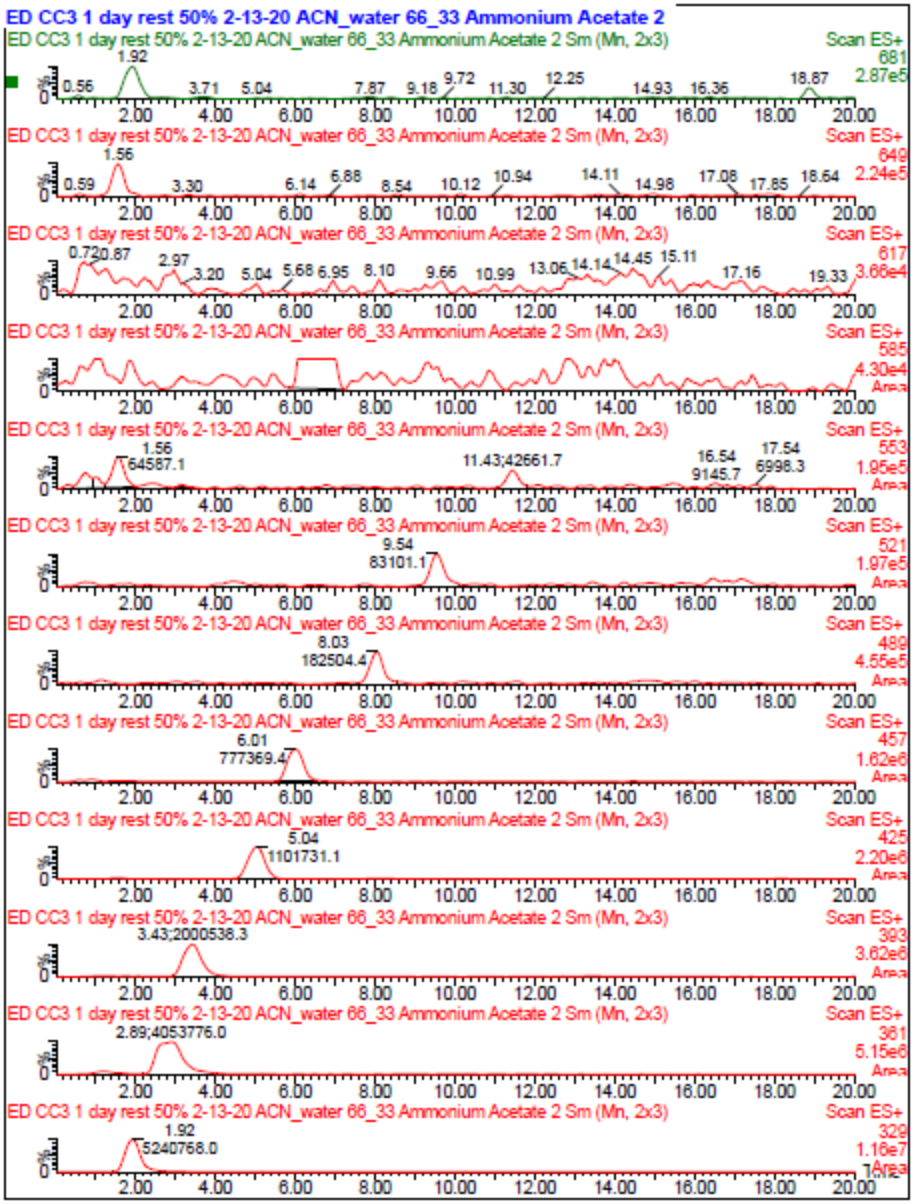


Figure A7. 200 mAh/g discharged, 24 h aged, sample #2.

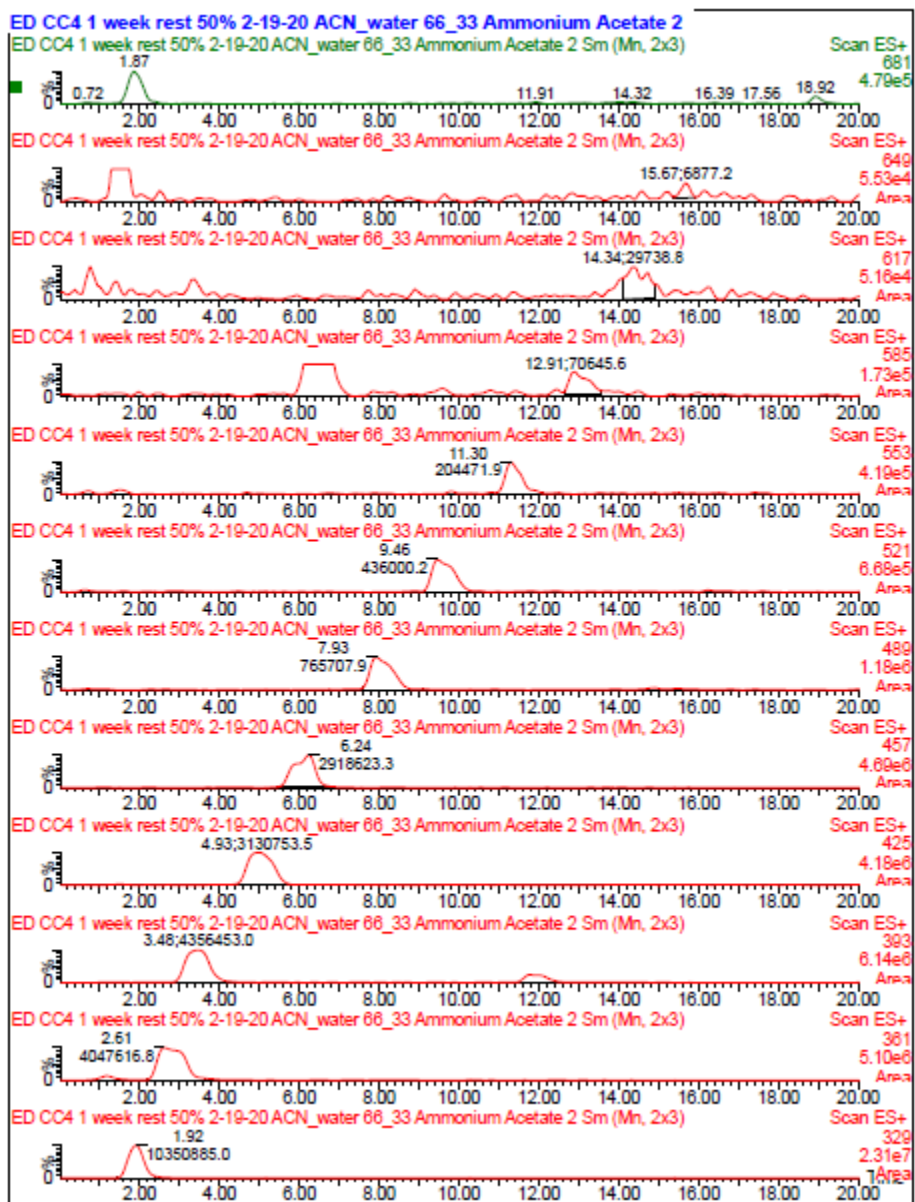


Figure A8. 200 mAh/g discharged, 1 week aged, sample #1.

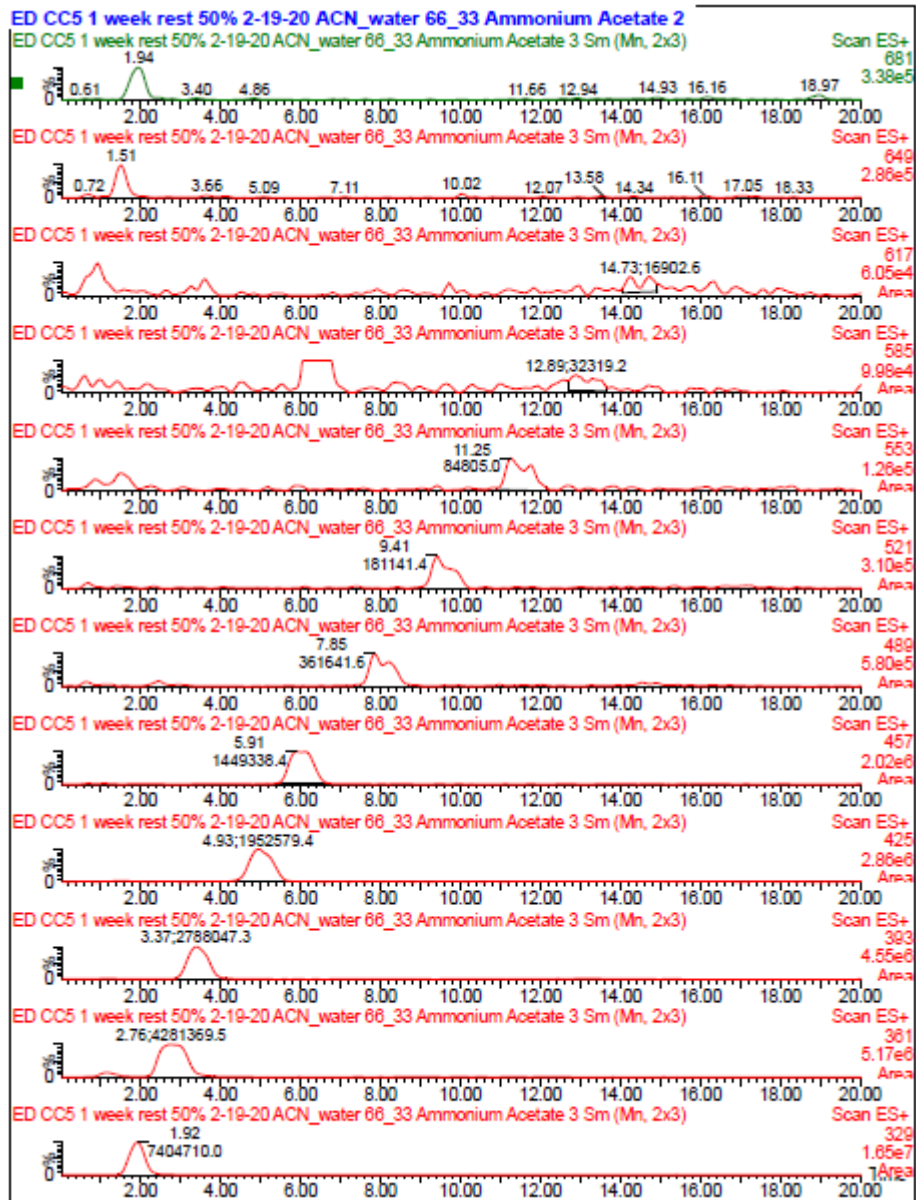


Figure A9. 200 mAh/g discharged, 1 week aged, sample #2.



Figure A10. 300 mAh/g discharged, no rest, sample #1.



Figure A11. 300 mAh/g discharged, no rest, sample #2.



Figure A12. 300 mAh/g discharged, 24 h aged, sample #1.



Figure A13. 300 mAh/g discharged, 24 h aged, sample #2.

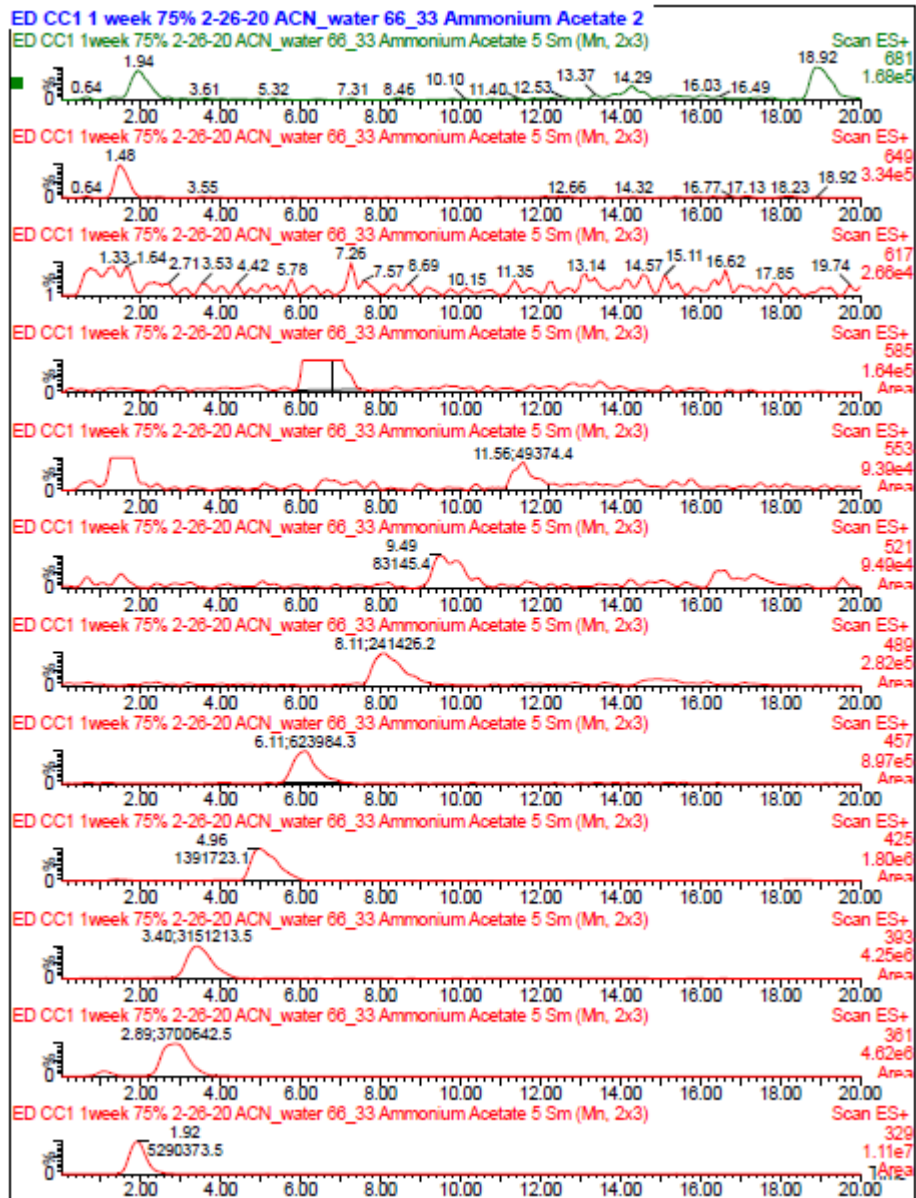


Figure A14. 300 mAh/g discharged, 1 week aged, sample #1.

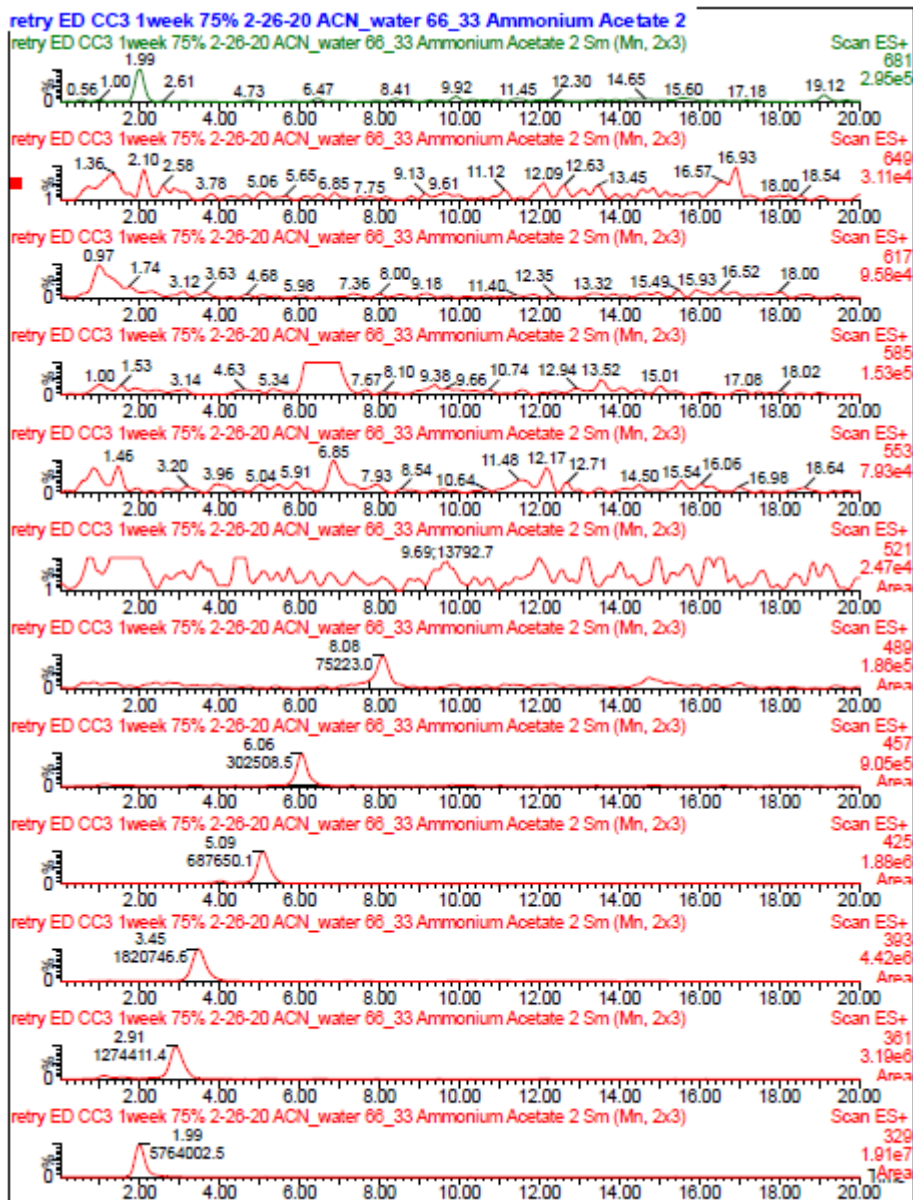


Figure A15. 300 mAh/g discharged, 1 week aged, sample #2.



Figure A16. 400 mAh/g discharged, no rest, sample #1.

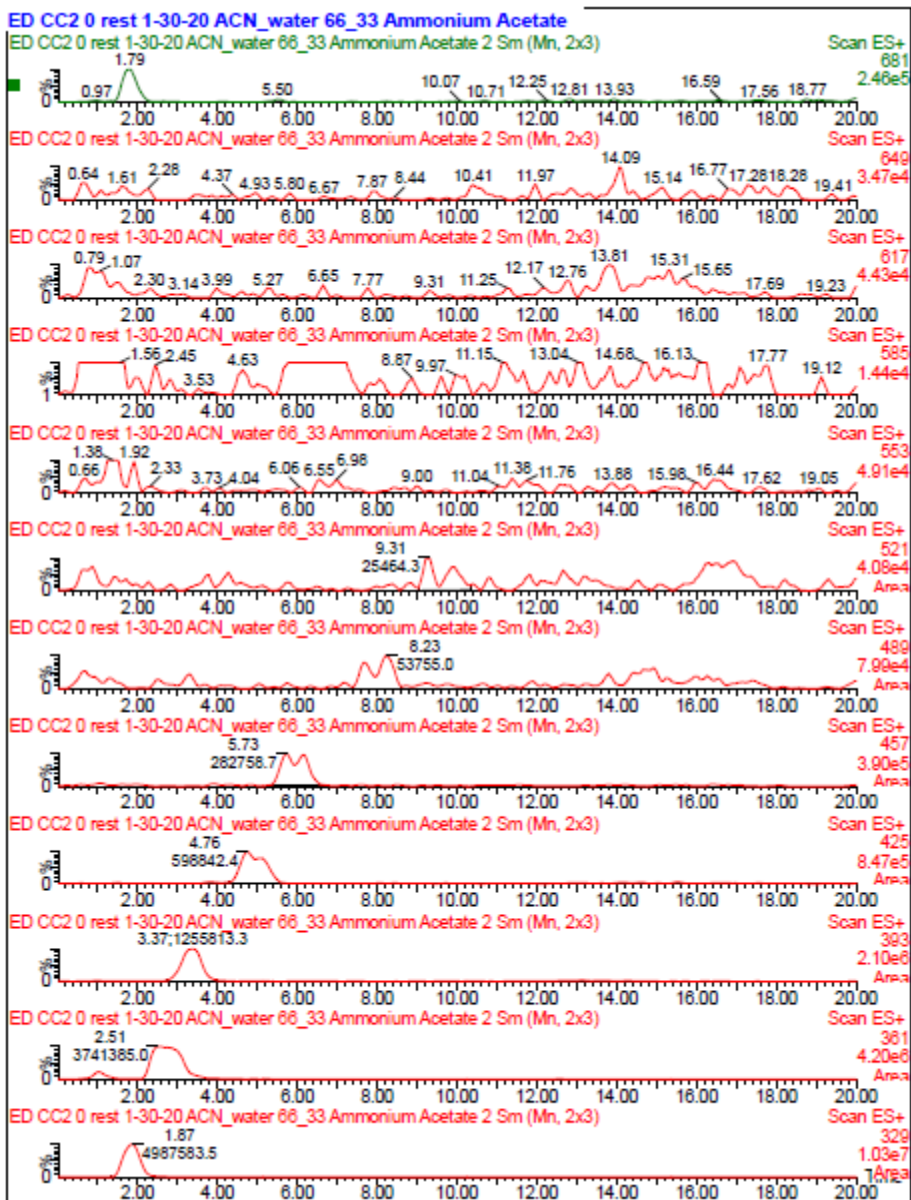


Figure A17. 400 mAh/g discharged, no rest, sample #2.

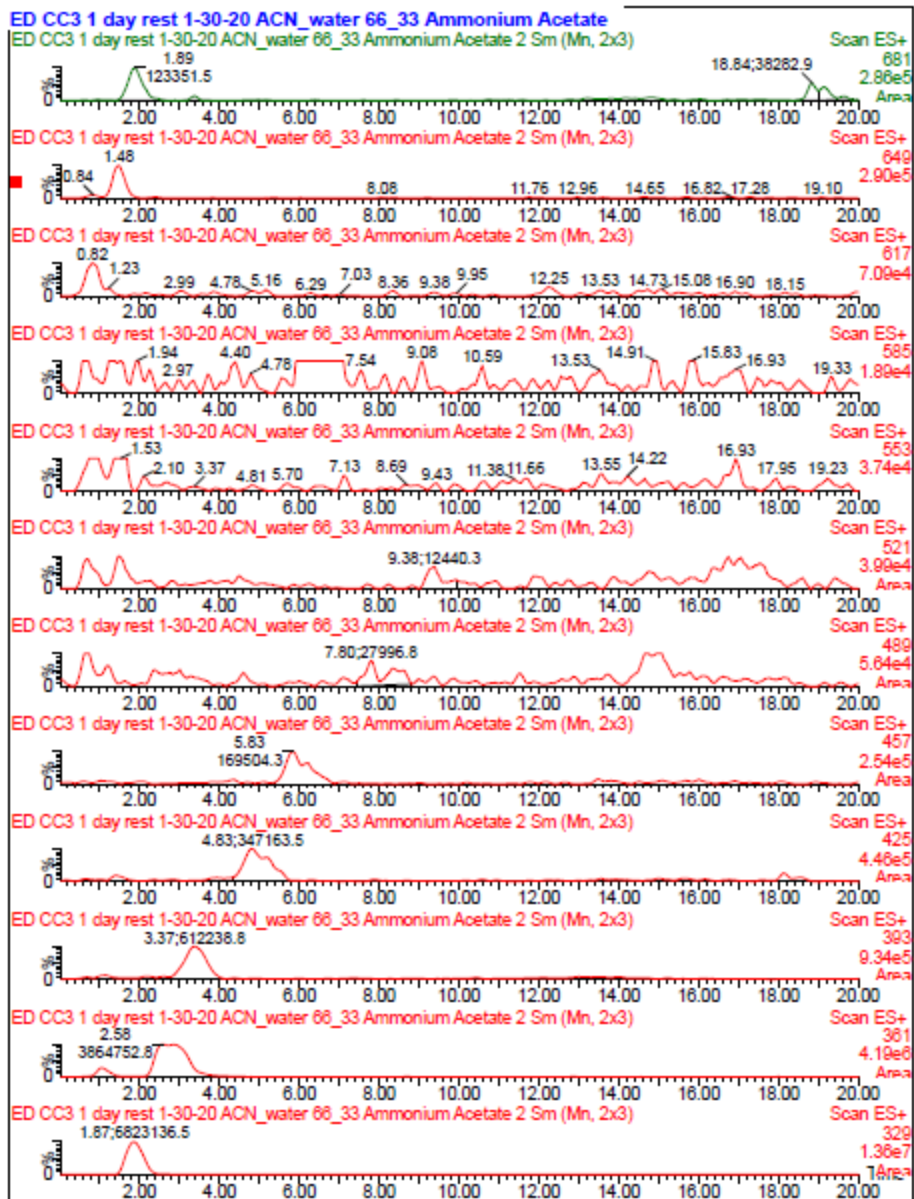


Figure A18. 400 mAh/g discharged, 24 h aged, sample #1.



Figure A19. 400 mAh/g discharged, 24 h aged, sample #2.

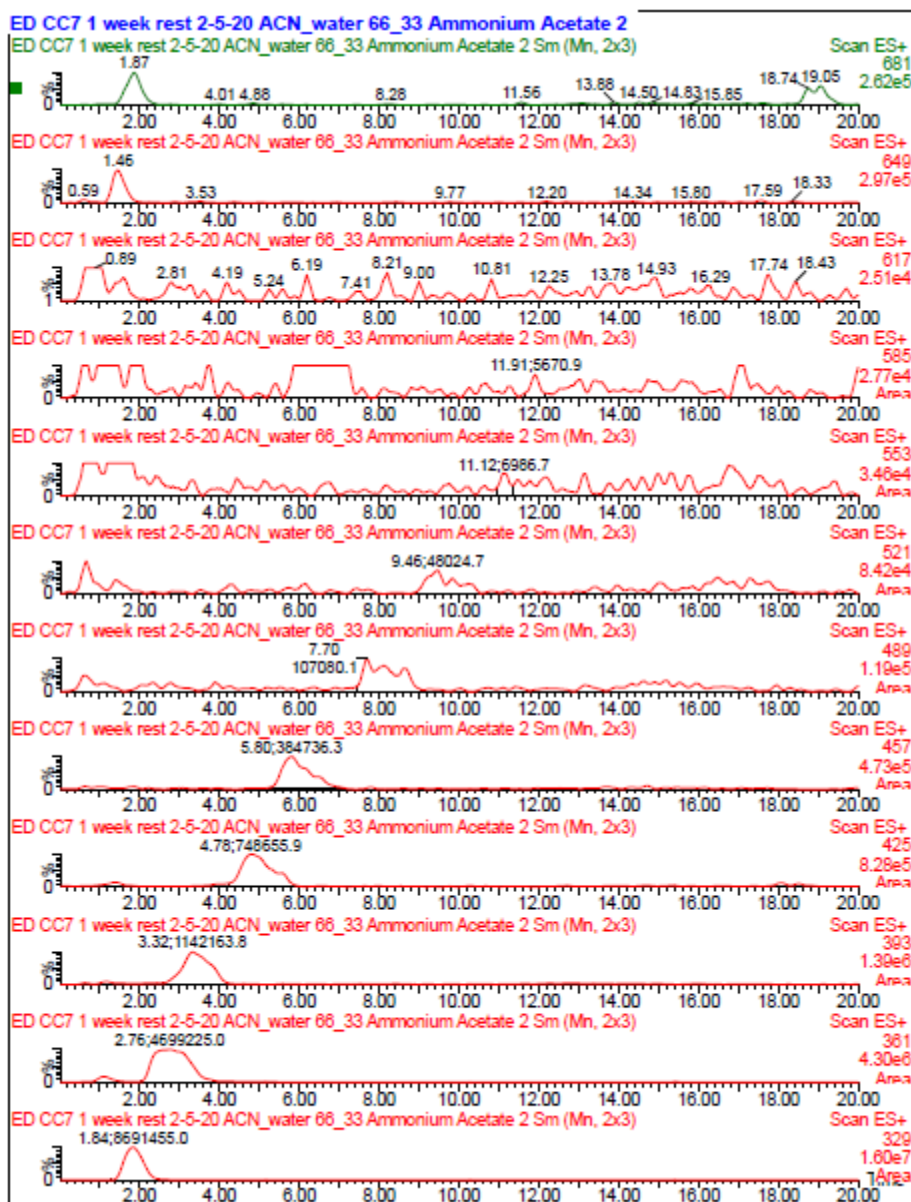


Figure A20. 400 mAh/g discharged, 1 week aged, sample #1.

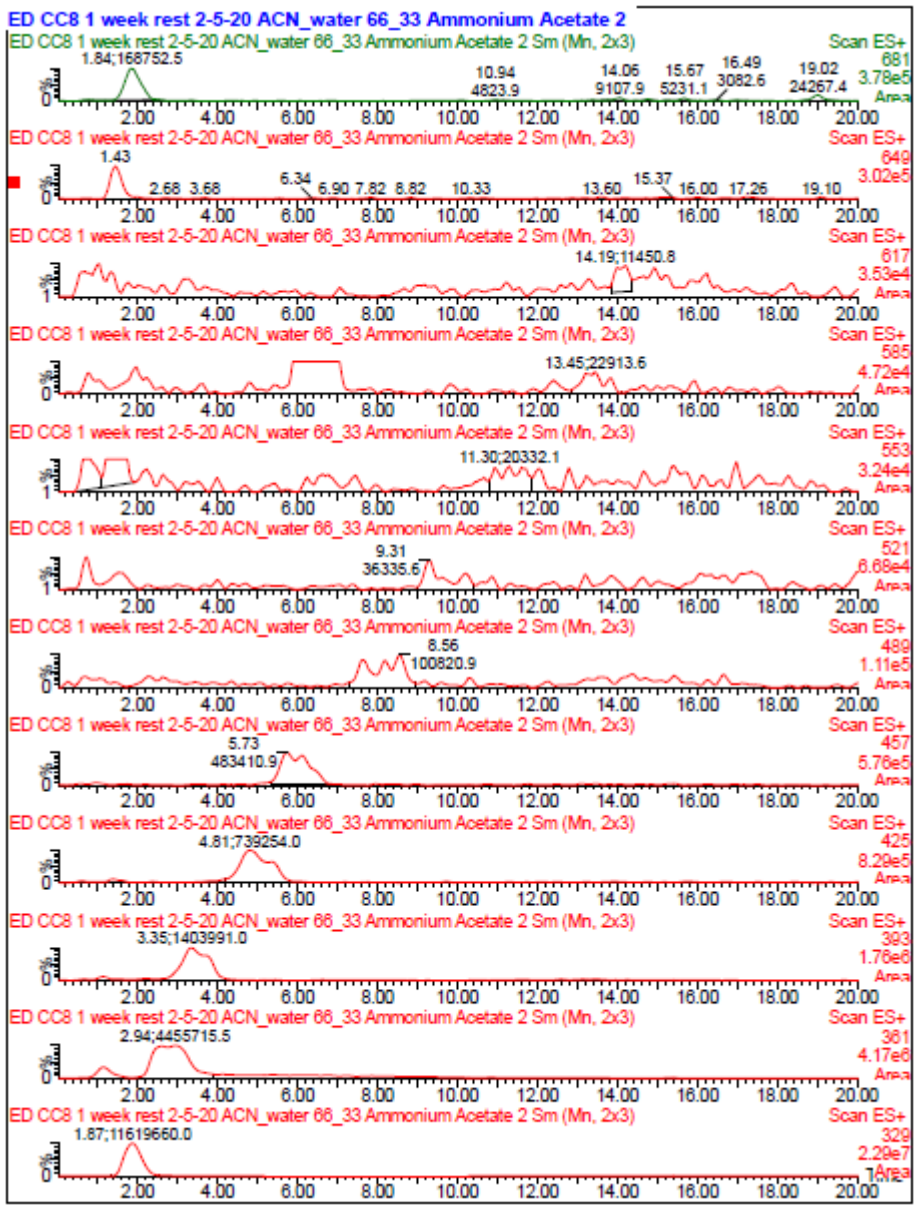


Figure A21. 400 mAh/g discharged, 1 week aged, sample #2.